Wigner surmise for mixed symmetry classes in random matrix theory

Sebastian Schierenberg, Falk Bruckmann, and Tilo Wettig

Institute for Theoretical Physics, University of Regensburg, 93040 Regensburg, Germany

We consider the nearest-neighbor spacing distributions of mixed random matrix ensembles interpolating between different symmetry classes or between integrable and nonintegrable systems. We derive analytical formulas for the spacing distributions of 2×2 or 4×4 matrices and show numerically that they provide very good approximations for those of random matrices with large dimension. This generalizes the Wigner surmise, which is valid for pure ensembles that are recovered as limits of the mixed ensembles. We show how the coupling parameters of small and large matrices must be matched depending on the local eigenvalue density.

I. INTRODUCTION

Random matrix theory (RMT) is a powerful mathematical tool which can be used to describe the statistical behavior of quantities arising in a wide variety of complex systems. It has been applied to many mathematical and physical problems with great success; see [1–3] for reviews. This wide range of applications is based on the fact that RMT describes universal quantities that do not depend on the detailed dynamical properties of a given system but rather are determined by global symmetries that are shared by all systems in a given symmetry class.

In RMT the operator governing the behavior of the system, such as the Hamilton or Dirac operator, is replaced by a random matrix with suitable symmetries. One then studies statistical properties of the eigenvalue spectrum of such random matrices, typically in the limit of large matrix dimension. To compare different systems in the same symmetry class with RMT, the eigenvalues of the physical system as well as those of the random matrices need to be "unfolded" [4]. The purpose of such an unfolding procedure is to separate the average behavior of the spectral density (which is not universal) from the spectral fluctuations (which are universal). Unfolding is essentially a local rescaling of the eigenvalues, resulting in an unfolded spectrum with mean level spacing equal to unity. How the rescaling is to be done is not unique and may depend on the system under study.

In this paper we focus on the so-called nearest-neighbor spacing distribution $P(s)$, i.e., the probability density to find two adjacent (unfolded) eigenvalues at a distance s. This quantity probes the strength of the eigenvalue repulsion due to interactions and can be computed analytically for the classical RMT ensembles, resulting in rather complicated expressions given in terms of prolate spheroidal functions [5]. However, it was realized early on that the level spacing distribution of large random matrices is very well approximated by that of 2×2 matrices in the same symmetry class.[1] For most practical purposes it is sufficient to use this so-called Wigner surmise [8] instead of the exact analytical result. It is given by

$$P_\beta(s) = a_\beta s^\beta e^{-b_\beta s^2}, \tag{1.1}$$

with $\beta = 1,2,4$ corresponding to the Gaussian orthogonal ensemble (GOE), Gaussian unitary ensemble (GUE), and Gaussian symplectic ensemble (GSE) of RMT, respectively. The quantities a_β and b_β are chosen such that

$$\int_0^\infty ds\, P_\beta(s) = 1 \quad \text{and} \quad \langle s \rangle = \int_0^\infty ds\, P_\beta(s)\, s = 1 \tag{1.2}$$

in all three cases. Explicit formulas will be given in Sec. II.

RMT describes quantum systems whose classical counterparts are chaotic [9] and correctly predicts the strong short-range correlations of the eigenvalues due to interactions. In contrast, the level spacing distribution of a quantum system whose classical counterpart is integrable is given by that of a Poisson process,

$$P_0(s) = e^{-s}, \tag{1.3}$$

corresponding to uncorrelated eigenvalues. We assign the Dyson index $\beta = 0$ to ensembles of this kind, which is a consistent extension of the generalized Gaussian ensembles with arbitrary real $\beta > 0$ introduced in Ref. [10].

Often physical systems consist of parts with different symmetries, or of a classically integrable and a chaotic part. Changing a parameter of the system may then result in transitions between different symmetry classes. Now, the question is whether a symmetry transition in a given physical system can be described by a transition between RMT ensembles (or Poisson). It has been shown in numerous studies that this is indeed the case. For example, billiards are showcases for the interplay of chaos and integrability, and certain billiards exhibit Poisson–GOE transitions [11–14]. A transition between GOE and GUE behavior takes place in the spectrum of a kicked top [15] or kicked rotor [16] when time-reversal symmetry is gradually broken. Furthermore, a transition from Poisson to GOE statistics was found for random points on fractals as the dimension is changed [17]. In the spectrum of the hydrogen atom in a magnetic field, transitions were observed from Poisson to GOE [18] as well as from GOE to GUE [19]. Transitions from Poisson to GOE or GUE statistics also occur in condensed matter physics, e.g., in the metal-insulator (Anderson) transition [20,21] whose properties are similar to those of the Brownian motion model introduced in Ref. [22]. In relativistic particle physics the Dirac operator shows transitions between different chiral symmetry classes [23] or an Anderson-type transition [24–26]. In the

---

[1]This does not work for non-Hermitian complex matrices [6,7].

spectra of nuclei a transition between GOE and Poisson spectral statistics takes place when levels sequences with different exact quantum numbers are mixed [4]. We thus conclude that RMT is broadly applicable not only to pure systems but also to mixed systems.

In this paper, we assume the Hamiltonian describing the mixed system to be of the form[2]

$$H = H_\beta + \lambda H_{\beta'}, \qquad (1.4)$$

where H_β represents the original system whose symmetry or integrability is broken by the perturbation $H_{\beta'}$ for small coupling parameter λ, and vice versa for large λ. For the quantities we analyze the absolute scale of H is irrelevant; only the relative scale between the different parts matters.

From the level statistics point of view, H_β and $H_{\beta'}$ correspond either to a Poisson process or to one of the three RMT ensembles. Hence, there are $\binom{4}{2} = 6$ possibilities for a transition between two of these four cases in Eq. (1.4), i.e., Poisson–GOE, Poisson–GUE, Poisson–GSE, GOE–GUE, GOE–GSE, and GUE–GSE. If a GSE matrix is involved in the transition, there are two possibilities for the other matrix: self-dual or not.[3] This leads to an even larger variety of mixed ensembles. Many transitions of this kind have been studied in earlier works, usually for large matrix dimension. Transitions between Gaussian ensembles are considered in Ref. [5], but closed forms for the spacing distribution could not be obtained, and self-dual symmetry was not conserved in the transitions involving the GSE. Mixtures of Gaussian ensembles with conserved self-dual symmetry and small matrix size are considered in Ref. [29], but only numerical results are given for the spacing distributions. Other examples include the heuristic Brody distribution [30] interpolating between Poisson and the GOE, the spacing distribution of a generalized Gaussian ensemble of 2×2 real random matrices [31], and a complete study of the transition between Poisson and the GUE [32]. The two-point correlation function of the latter case is also studied in Ref. [33].

Note that an exact analytical calculation of $P(s)$ for systems described by an ansatz of the form (1.4) is much harder than, e.g., the analytical calculation of low-order spectral correlation functions, which are already difficult to obtain. Here, we do not attempt an analytical calculation of $P(s)$ for large matrix dimension. Rather, motivated by the reliability of the Wigner surmise, we study the possible transitions in Eq. (1.4) for 2×2 matrices (or, in the symplectic case, 4×4 matrices, because the smallest nontrivial self-dual matrix has this size) and compare the resulting level spacing distributions with that of large random matrices, the latter obtained numerically. The cases of Poisson–GOE and GOE–GUE were worked out earlier by Lenz and Haake [15], and the spacing distribution of a 2×2 matrix interpolating between Poisson and GUE is given in Ref. [34]. These cases will briefly be reviewed below, and the remaining ones are the main subject of this work.

---

[2]Other possibilities have also been investigated (see, e.g., [5,27,28]) but will not be considered in this paper.

[3]An even-dimensional matrix A is called self-dual if $J A^T J^T = A$, with J given in Eq. (G4).

This paper is organized as follows. In Sec. II we derive analytical results for $P(s)$ for small matrix sizes. If $H_{\beta'}$ is from the GSE (i.e., $H_{\beta'}$ is self-dual) we construct in Secs. II D, II F, and II G self-dual matrices H_β to maintain the Kramers degeneracy. In Sec. II H we consider the case where a 4×4 GSE matrix is perturbed by a non-self-dual GUE matrix. Section III provides strong numerical evidence that the results obtained in Sec. II approximate the spacing distributions of large random matrices very well. We give a perturbative argument for the matching of the couplings used for the Wigner surmise and for large matrices, respectively, and derive an approximate result that involves the eigenvalue density. This result describes the numerical data rather well. We also show that the transitions from the GSE to either a non-self-dual Poissonian ensemble or the GOE proceed via an intermediate transition to the GUE and can also be described by the surmises calculated in Sec. II. We summarize our findings and conclude in Sec. IV. Technical details are worked out in several Appendices.

II. SPACING DISTRIBUTIONS FOR SMALL MATRICES

A. Preliminaries

In the spirit of the Wigner surmise, we now calculate the distributions $P(s)$ of eigenvalue spacings s of mixed ensembles for the smallest nontrivial (i.e., 2×2 or 4×4) matrices, with $P(s)$ normalized as in Eq. (1.2). Unfolding is not needed for these matrices since they have only two independent eigenvalues (except for Sec. II H). We first study the transitions from the integrable to the chaotic case for the three Gaussian ensembles and then proceed to the transitions between different symmetry classes.

We define the 2×2 Poisson process by a matrix

$$H_0 = \begin{pmatrix} 0 & 0 \\ 0 & p \end{pmatrix}, \qquad (2.1)$$

where p is a Poisson distributed non-negative random number with unit mean value; i.e., its probability density is $P_0(p) = e^{-p}$. The eigenvalue spacing of this matrix is obviously Poissonian, as the spacing is just p, and therefore we obtain Eq. (1.3).

The choice of H_0 may look like a special case, but it suffices for our purposes. The most general Hermitian 2×2 matrix with spacing p can be obtained from Eq. (2.1) by a common shift of the eigenvalues (which does not influence the spacing) and a basis transformation. This transformation can be absorbed in the perturbing matrix since it does not change the probability distribution of the latter. To see this, suppose we had started with a general nondiagonal H_0, also with eigenvalues 0 and p, instead of Eq. (2.1). When added to a random matrix $H_{\beta'}$ with $\beta' = 1,2,4$, we choose it to be real symmetric, Hermitian, or self-dual, respectively, in order to preserve the symmetry properties of $H_{\beta'}$. Then H_0 is diagonalized by a suitable matrix Ω; i.e., $\mathrm{diag}(0,p) = \Omega^{-1} H_0 \Omega$, where Ω is orthogonal ($\beta = 1$), unitary ($\beta = 2$), or symplectic ($\beta = 4$). In the total matrix H this is equivalent to $\Omega^{-1} H_{\beta'} \Omega$ perturbing $\mathrm{diag}(0,p)$, but the probability distribution of the perturbation is invariant under the transformation Ω.

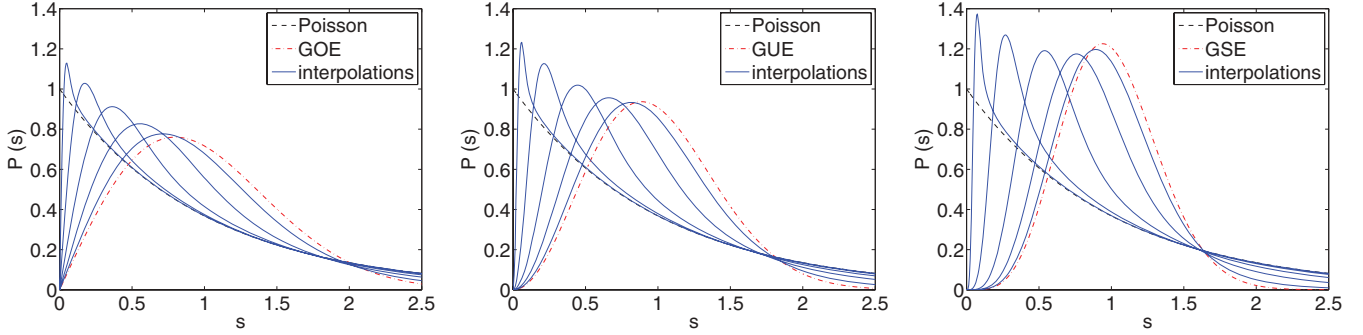For matrices $H_{1,2,4}$ from the GOE, GUE, and GSE, respectively, we choose the mean values of the matrix elements

FIG. 1. (Color online) Spacing distributions $P_{0\to\beta'}(s;\lambda)$ of the transitions Poisson $\to$ GOE [left, Eq. (2.4)], GUE [middle, Eq. (2.12)] and GSE [right, Eq. (2.26)] for 2×2 or 4×4 matrices with coupling parameters $\lambda = 0.02, 0.08, 0.2, 0.4,$ and 0.8 (maxima moving from left to right as λ increases). In the GSE case the matrix representing the Poisson process was made self-dual. All formulas were verified by comparison to numerically obtained spacing distributions of 2×2 or 4×4 random matrices.

to be 0 and the normalization

$$\langle [(H_{1,2,4})_{ii}]^2 \rangle = 2 \left\langle \left[\left(H_{1,2,4}^{(\nu)} \right)_{i\neq j} \right]^2 \right\rangle = 1. \quad (2.2)$$

The index $\nu = 0, \ldots, \beta - 1$ distinguishes the components of the complex GUE or quaternion GSE matrix elements, while the GOE matrix elements possess only a real part.

All results we derive from Eq. (1.4) will be symmetric in λ since the distribution of the elements of $H_{\beta'}$ is symmetric about zero (the perturbation will be taken from one of the Gaussian ensembles in each case). This means that our results should be expressed in terms of $|\lambda|$. To avoid such cumbersome notation we restrict ourselves to non-negative λ.

B. Poisson to GOE

We first consider the case that corresponds to a classically integrable system perturbed by a chaotic part with antiunitary symmetry squaring to $\mathbb{1}$. The integrable part is represented by a Poisson process, and the chaotic one by the GOE. The spacing distribution for this case has been derived in Ref. [15], and we state it here for the sake of completeness.

The 2×2 random matrix

$$H = H_0 + \lambda H_1 = \begin{pmatrix} 0 & 0 \\ 0 & p \end{pmatrix} + \lambda \begin{pmatrix} a & c \\ c & b \end{pmatrix} \quad (2.3)$$

consists of H_0 from (2.1) and H_1 from the GOE, i.e., a real symmetric matrix with normalization given in Eq. (2.2). The calculations are very similar to the ones for the transition from Poisson to the GSE, which are presented in Sec. II D (see also Appendix A). The resulting spacing distribution of H reads

$$P_{0\to 1}(s;\lambda) = Cs\, e^{-D^2 s^2} \int_0^\infty dx\, e^{-\frac{x^2}{4\lambda^2} - x} I_0\left(\frac{xDs}{\lambda}\right), \quad (2.4)$$

with

$$D(\lambda) = \frac{\sqrt{\pi}}{2\lambda} U\left(-\frac{1}{2}, 0, \lambda^2\right), \quad (2.5)$$

$$C(\lambda) = 2D(\lambda)^2, \quad (2.6)$$

where U is the Tricomi confluent hypergeometric function (or Kummer function) [[35], Eq. (13.1.3)] and I_0 is a modified Bessel function [[35], Eq. (9.6.3)]. $P_{0\to 1}(s;\lambda)$ is plotted in Fig. 1 (left) for various values of λ. The formula is equivalent

to the one given in Ref. [15], but our integration variable x is scaled differently.

In the limiting cases of $\lambda \to 0$ and $\lambda \to \infty$ we have

$$D(\lambda) \sim \begin{cases} 1/(2\lambda) & \text{for } \lambda \to 0, \\ \sqrt{\pi}/2 & \text{for } \lambda \to \infty. \end{cases} \quad (2.7)$$

Using the asymptotic expansion of the Bessel function, it is straightforward to show that for $\lambda \to 0$ we obtain the Poisson result e^{-s}. It is even simpler to show that the Wigner surmise $(\pi s/2)\, e^{-\pi s^2/4}$ for the GOE is obtained for $\lambda \to \infty$.

The small-s behavior of $P_{0\to 1}(s;\lambda)$ shows interesting features. To investigate this behavior, we consider separately the cases $\lambda = 0$ and $\lambda > 0$. For $\lambda = 0$ we have by construction

$$P_{0\to 1}(s;0) = e^{-s} = 1 - s + O(s^2). \quad (2.8)$$

For $\lambda > 0$ we obtain from Eq. (2.4)

$$P_{0\to 1}(s;\lambda) = c(\lambda)s + O(s^3), \quad (2.9)$$

with

$$c(\lambda) \sim \frac{\sqrt{\pi}}{2\lambda} \quad \text{for } \lambda \to 0, \quad (2.10)$$

which means that we recover the linear level repulsion of the GOE for arbitrarily small λ, i.e., for arbitrarily small admixture of the chaotic part as also observed in Refs. [36–38]. This implies that for $\lambda \to 0$ the distribution, viewed as a function of λ, develops a discontinuity at $s = 0$, since $P_{0\to 1}(s = 0; \lambda = 0) = 1$ while $P_{0\to 1}(s = 0; \lambda > 0) = 0$. This effect is clearly seen in Fig. 1 (left).

For small values of λ and s, we observe something reminiscent of the Gibbs phenomenon, i.e., the interpolation overshoots the Poisson curve considerably. In the limit of $\lambda \to 0$, one can show (see Appendix B 2) that the maximum of $P_{0\to 1}$ is at $s_{max} = 2.51393\lambda$ with a finite value of $P_{0\to 1}(s_{max}; \lambda \to 0) = 1.17516$. This implies an overshoot of 17.5% compared to the Poisson curve. Such an effect also occurs in the transitions from Poisson to GUE and GSE that are treated in Secs. II C and II D below, with, respectively, quadratic and quartic level repulsion in the small-s regime.

The large-s behavior of $P_{0\to 1}(s;\lambda)$ is analyzed in Appendix A, and we obtain Poisson-like behavior for any finite λ [see Eq. (A7)]. This is in contrast to the small-s behavior, which is GOE-like for any nonzero λ.

C. Poisson to GUE

We now consider the transition from Poisson to the GUE. This corresponds to a classically integrable system with a chaotic perturbation without antiunitary symmetry. The 2×2 random matrix

$$H = H_0 + \lambda H_2 = \begin{pmatrix} 0 & 0 \\ 0 & p \end{pmatrix} + \lambda \begin{pmatrix} a & c_0 + ic_1 \\ c_0 - ic_1 & b \end{pmatrix} \tag{2.11}$$

contains H_2 from the GUE, i.e., a complex Hermitian matrix with normalization (2.2). The spacing distribution of an equivalent setup with different normalizations of the random matrix elements was already considered in Ref. [34], so we just state the result,

$$P_{0\to 2}(s; \lambda) = Cs^2 e^{-D^2 s^2} \int_0^\infty dx\, e^{-\frac{x^2}{4\lambda^2} - x} \frac{\sinh z}{z}, \tag{2.12}$$

with $z = xDs/\lambda$ and

$$D(\lambda) = \frac{1}{\sqrt{\pi}} + \frac{1}{2\lambda} e^{\lambda^2} \operatorname{erfc}(\lambda) - \frac{\lambda}{2} \operatorname{Ei}(\lambda^2)$$
$$+ \frac{2\lambda^2}{\sqrt{\pi}} \,{}_2F_2\left(\frac{1}{2}, 1; \frac{3}{2}, \frac{3}{2}; \lambda^2\right), \tag{2.13}$$

$$C(\lambda) = \frac{4D(\lambda)^3}{\sqrt{\pi}}. \tag{2.14}$$

Here, erfc is the complementary error function [[35], Eq. (7.1.2)], Ei is the exponential integral [[35], Eq. (5.1.2)], and ${}_2F_2$ is a generalized hypergeometric function [39, Eq. (9.14.1)]. We could also have written the result in the form of Eqs. (A2) and (A3) since $\sinh z = \sqrt{\pi z/2}\, I_{1/2}(z)$.

To check the validity of Eq. (2.12) and to see the emergence of the limiting spacing distributions, we now consider the limits $\lambda \to 0$ and $\lambda \to \infty$. First note that for $\lambda \to 0$ we have

$$D \sim \frac{1}{2\lambda} \quad \text{and} \quad C \sim \frac{1}{2\lambda^3 \sqrt{\pi}} \tag{2.15}$$

so that Eq. (2.12) becomes for $s > 0$

$$P_{0\to 2}(s; 0) = \lim_{\lambda \to 0} \frac{s^2}{2\lambda^3 \sqrt{\pi}} \int_0^\infty dx\, e^{-\frac{1}{4\lambda^2}(s^2 + x^2) - x} \frac{\sinh z}{z}$$
$$= \frac{s}{2\sqrt{\pi}} \int_0^\infty dx\, \frac{e^{-x}}{x} \underbrace{\lim_{\lambda \to 0} \frac{1}{\lambda}\left(e^{-\frac{(s-x)^2}{4\lambda^2}} - e^{-\frac{(s+x)^2}{4\lambda^2}}\right)}_{=2\sqrt{\pi}[\delta(s-x) - \delta(s+x)]}$$
$$= e^{-s}, \tag{2.16}$$

which is the Poisson distribution as required. For $\lambda \to \infty$ we have

$$D \sim \frac{2}{\sqrt{\pi}} \quad \text{and} \quad C \sim \frac{32}{\pi^2} \tag{2.17}$$

so that Eq. (2.12) becomes

$$P_{0\to 2}(s; \infty) = \frac{32 s^2}{\pi^2} e^{-\frac{4s^2}{\pi}} \lim_{\substack{\lambda \to \infty \\ z \to 0}} \int_0^\infty dx\, e^{-\frac{x^2}{4\lambda^2} - x} \frac{\sinh z}{z}$$
$$= \frac{32 s^2}{\pi^2} e^{-\frac{4s^2}{\pi}}, \tag{2.18}$$

which is the Wigner surmise for the GUE.

The integral in Eq. (2.12) can be computed numerically without difficulties as the integrand decays like a Gaussian for large x and becomes constant for small x.[4] The resulting distribution $P_{0\to 2}(s; \lambda)$ is plotted in Fig. 1 (middle).

As in Sec. II B, a discontinuity is found at $s = 0$ toward the Poisson result. For $\lambda > 0$ we obtain from Eq. (2.12)

$$P_{0\to 2}(s; \lambda) = c(\lambda)s^2 + O(s^4), \tag{2.19}$$

with

$$c(\lambda) \sim \frac{1}{2\lambda^2} \quad \text{for} \quad \lambda \to 0. \tag{2.20}$$

Hence we obtain the quadratic level repulsion of the GUE for arbitrarily small coupling parameter. For $\lambda \to 0$, the maximum of the function is at $s_{\max} = 3.00395\,\lambda$, with a value of $P_{0\to 2}(s_{\max}; \lambda \to 0) = 1.28475$ (see Appendix B 2).

The large-s behavior of $P_{0\to 2}(s; \lambda)$ is given by Eq. (A7); i.e., it is Poisson-like.

D. Poisson to GSE

In this case, a classically integrable system is perturbed by a chaotic part with antiunitary symmetry squaring to $-\mathbb{1}$ and hence represented by the self-dual matrices of the GSE. One has to consider 4×4 matrices here, because a self-dual 2×2 matrix is proportional to $\mathbb{1}_2$ and has only one nondegenerate eigenvalue. As mentioned in Sec. I, there are now two possibilities: The Poisson process could be represented by a self-dual or a non-self-dual matrix. Here we only consider the former possibility, while the latter will be discussed in Sec. III E. A self-dual Poisson matrix is obtained by taking a tensor product of Eq. (2.1) with $\mathbb{1}_2$. Thus the transition matrix is

$$H = H_0 \otimes \mathbb{1}_2 + \lambda H_4 = \begin{pmatrix} 0 & 0 & 0 & 0 \\ 0 & 0 & 0 & 0 \\ 0 & 0 & p & 0 \\ 0 & 0 & 0 & p \end{pmatrix}$$
$$+ \lambda \begin{pmatrix} a & 0 & c_0 + ic_3 & c_1 + ic_2 \\ 0 & a & -c_1 + ic_2 & c_0 - ic_3 \\ c_0 - ic_3 & -c_1 - ic_2 & b & 0 \\ c_1 - ic_2 & c_0 + ic_3 & 0 & b \end{pmatrix}, \tag{2.21}$$

where the GSE matrix H_4 is Hermitian and self-dual, and can be represented by a 2×2 matrix whose elements are real quaternions (see [5] for details).

We now explain the calculation of the spacing distribution for this transition. The computation of the previous cases, Poisson to GOE and Poisson to GUE, can be done in a similar fashion.

––––––––––

[4]Note that the integral can be expressed in terms of imaginary error functions, but for increasing s delicate cancellations occur that make it impractical to use this form for numerical evaluation. This is why we present Eq. (2.12) as the final formula, which is well suited for numerical integration.

Due to the self-dual structure of H, the spacing S between its nondegenerate eigenvalues can be computed analytically and reads

$$S = \lambda \sqrt{(a - b - p/\lambda)^2 + 4c_\mu c_\mu}, \qquad (2.22)$$

where the repeated index μ indicates a sum from 0 to 3. We have intentionally written S instead of s since we eventually need to rescale the spacing to ensure $\langle s \rangle = 1$. The desired spacing distribution is proportional to the integral

$$I(S) = \int dp \, da \, db \prod_{\nu=0}^{3} dc_\nu \, P_0(p) P_a(a) P_b(b) P_{c_\nu}(c_\nu)$$
$$\times \delta\left(S - \sqrt{[a - (b + p/\lambda)]^2 + 4c_\mu c_\mu}\right), \qquad (2.23)$$

where we have rescaled S by λ for simplicity and are not yet concerned with the normalization. The distributions $P_\alpha(\alpha)$ of the random variables $\alpha = a, b, c_0, c_1, c_2, c_3$ are Gaussian, with variances given by Eq. (2.2),

$$\sigma_{a,b}^2 = 2\sigma_{c_0, c_1, c_2, c_3}^2 = 1. \qquad (2.24)$$

Inserting this into Eq. (2.23) and shifting $b \to b - p/\lambda$ gives

$$I(S) \propto \int_0^\infty dp \int_{-\infty}^\infty da \, db \prod_{\nu=0}^{3} dc_\nu \, e^{-p - \frac{1}{2}a^2 - \frac{1}{2}(b - p/\lambda)^2 - c_\mu c_\mu}$$
$$\times \delta\left(S - \sqrt{(a - b)^2 + 4c_\mu c_\mu}\right). \qquad (2.25)$$

The multidimensional integral in this expression is computed in Appendix C 1. Rescaling the spacing and normalizing the distribution to satisfy Eq. (1.2), we obtain

$$P_{0 \to 4}(s; \lambda) = Cs^4 e^{-D^2 s^2} \int_0^\infty dx \, e^{-\frac{x^2}{4\lambda^2} - x} \frac{z \cosh z - \sinh z}{z^3}, \qquad (2.26)$$

with $z = x D s / \lambda$ and

$$D(\lambda) = \frac{\lambda}{2\sqrt{\pi}} \int_0^\infty dx \, e^{-2\lambda x}$$
$$\times \frac{(4x^3 + 2x)e^{-x^2} + \sqrt{\pi}(4x^4 + 4x^2 - 1)\,\mathrm{erf}(x)}{x^3}, \qquad (2.27)$$

$$C(\lambda) = \frac{8D(\lambda)^5}{\sqrt{\pi}}, \qquad (2.28)$$

where erf is the error function [[35], Eq. (7.1.1)]. The last term in the integrand of Eq. (2.26) is proportional to $I_{3/2}(z)$, in agreement with Eqs. (A2) and (A3).

In the limiting cases of $\lambda \to 0$ and $\lambda \to \infty$ we find

$$D(\lambda) \sim \begin{cases} 1/(2\lambda) & \text{for } \lambda \to 0, \\ 8/(3\sqrt{\pi}) & \text{for } \lambda \to \infty. \end{cases} \qquad (2.29)$$

For $\lambda \to 0$, manipulations analogous to those performed in Eq. (2.16) lead to the Poisson result e^{-s}. For $\lambda \to \infty$ the integral in Eq. (2.26) becomes trivial and yields $1/3$ so that we obtain the Wigner surmise $(64/9\pi)^3 s^4 e^{-64s^2/9\pi}$ for the GSE.

Equation (2.26) is plotted in Fig. 1 (right) and again displays a discontinuity at $s = 0$ as $\lambda \to 0$. For $\lambda > 0$ we now have

$$P_{0 \to 4}(s; \lambda) = c(\lambda)s^4 + O(s^6), \qquad (2.30)$$

with

$$c(\lambda) \sim \frac{1}{12\lambda^4} \quad \text{for } \lambda \to 0. \qquad (2.31)$$

For $\lambda \to 0$, the maximum of the function is at $s_{\max} = 3.76023\,\lambda$, with a value of $P_{0 \to 4}(s_{\max}; \lambda \to 0) = 1.43453$ (see Appendix B 2).

The large-s behavior of $P_{0 \to 4}(s; \lambda)$ is again Poisson-like and given by Eq. (A7).

E. GOE to GUE

With this section we start the investigation of transitions between different chaotic ensembles using the smallest possible matrix size.

We consider the 2×2 matrix

$$H = H_1 + \lambda H_2. \qquad (2.32)$$

The spacing distribution for this transition was already computed in Ref. [15]. With the normalization of ensembles given in Eq. (2.2), it reads

$$P_{1 \to 2}(s; \lambda) = Cs \, e^{-D^2 s^2} \, \mathrm{erf}\left(\frac{Ds}{\lambda}\right), \qquad (2.33)$$

with

$$D(\lambda) = \frac{\sqrt{1 + \lambda^2}}{\sqrt{\pi}} \left(\frac{\lambda}{1 + \lambda^2} + \mathrm{arccot}\,\lambda\right), \qquad (2.34)$$

$$C(\lambda) = 2\sqrt{1 + \lambda^2}\,D(\lambda)^2. \qquad (2.35)$$

This formula matches the result of [15] up to a rescaling of the coupling parameter λ by a factor of $\sqrt{2}$, which is due to a different normalization of the ensembles used there.

In the limiting cases of $\lambda \to 0$ and $\lambda \to \infty$ we have

$$D(\lambda) \sim \begin{cases} \sqrt{\pi}/2 & \text{for } \lambda \to 0, \\ 2/\sqrt{\pi} & \text{for } \lambda \to \infty. \end{cases} \qquad (2.36)$$

For $\lambda \to 0$, the error function in Eq. (2.33) can be replaced by unity (for $s > 0$), and we obtain the Wigner surmise for the GOE. For $\lambda \to \infty$, using the first-order Taylor expansion of the error function yields the Wigner surmise for the GUE.

The result (2.33) is plotted in Fig. 2 (left). In the small-s region, we now have for $\lambda > 0$

$$P_{1 \to 2}(s; \lambda) = c(\lambda)s^2 + O(s^4), \qquad (2.37)$$

with

$$c(\lambda) \sim \frac{\pi}{2\lambda} \quad \text{for } \lambda \to 0. \qquad (2.38)$$

Similar to the previous sections, a nonanalytic transition between weaker and stronger level repulsion develops as $\lambda \to 0$, except that now there is no jump in the function itself but rather in its derivative at $s = 0$. Therefore, the stronger level repulsion takes over immediately in the small-s regime, if $\lambda > 0$. As we shall see below, this also happens in the remaining transitions, GOE to GSE and GUE to GSE, and seems to be a characteristic feature of the mixed ensembles.

The large-s behavior of $P_{1 \to 2}(s; \lambda)$ is obtained immediately from Eq. (2.33) by noticing that $\mathrm{erf}(x) \to 1$ for $x \to \infty$. In analogy to the transitions from Poisson to RMT this implies that the large-s behavior is dominated by the ensemble with the smaller β.

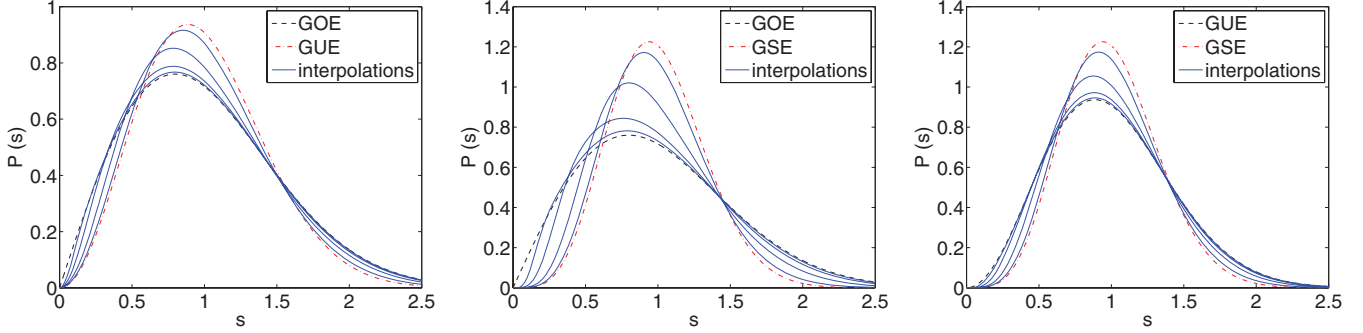FIG. 2. (Color online) Spacing distributions $P_{\beta \to \beta'}(s; \lambda)$ of the transitions GOE $\to$ GUE [left, Eq. (2.33)], GOE $\to$ GSE [middle, Eq. (2.41)], and GUE $\to$ GSE [right, Eq. (2.52)] for 2×2 or 4×4 matrices with coupling parameters $\lambda = 0.1, 0.2, 0.4$, and 0.8 (maxima increasing with λ). In the cases involving the GSE, the GOE or GUE matrices were made self-dual. All formulas were verified by comparison to numerically obtained spacing distributions of 2×2 or 4×4 random matrices.

F. GOE to GSE

As the GSE is involved in this transition, we need matrices of size 4×4. Again there are two possibilities: The GOE matrix could be made self-dual, or it could be non-self-dual (as it generically is). Here we only consider the former case, while the latter case will be discussed in Sec. III E. As in Ref. [29] we define a modified GOE matrix by

$$
H_1 \otimes \mathbb{1}_2 = \begin{pmatrix} a & 0 & c & 0 \\ 0 & a & 0 & c \\ c & 0 & b & 0 \\ 0 & c & 0 & b \end{pmatrix}, \qquad (2.39)
$$

with real parameters a, b, and c. This matrix is self-dual, so we can add it to a matrix from the GSE without spoiling the symmetry properties of the latter. Thus we consider

$$
H = H_1 \otimes \mathbb{1}_2 + \lambda H_4, \qquad (2.40)
$$

where H_1 and H_4 are normalized according to Eq. (2.2). The eigenvalues of the sum are doubly degenerate and can be calculated easily due to self-duality.

After some algebra (see Appendix C 2) we obtain for the spacing distribution of H,

$$
P_{1 \to 4}(s; \lambda) = C s^4 e^{-(1+2\lambda^2) D^2 s^2} \int_0^1 dx\, (1 - x^2)\, e^{(xDs)^2}
$$
$$
\times [I_0(z) - I_1(z)], \qquad (2.41)
$$

where $z = (1 - x^2) D^2 s^2$, I_0 and I_1 are modified Bessel functions, and

$$
D(\lambda) = \frac{\lambda - \lambda^3 + (1 + \lambda^2)^2 \operatorname{arccot}\lambda}{\sqrt{2\pi}\, \lambda \sqrt{1 + \lambda^2}}, \qquad (2.42)
$$

$$
C(\lambda) = \frac{2^{9/2}}{\sqrt{\pi}} \lambda^2 (1 + \lambda^2)^{3/2} D(\lambda)^5. \qquad (2.43)
$$

In the limiting cases of $\lambda \to 0$ and $\lambda \to \infty$ we have

$$
D(\lambda) \sim \begin{cases} \sqrt{\pi}/(2^{3/2}\lambda) & \text{for } \lambda \to 0, \\ 8/(3\sqrt{2\pi}\lambda) & \text{for } \lambda \to \infty. \end{cases} \qquad (2.44)
$$

For $\lambda \to 0$, we use the asymptotic expansion of the Bessel functions to simplify the integral over x in Eq. (2.41) and obtain the Wigner surmise for the GOE. For $\lambda \to \infty$, the exponential

and the difference of the Bessel functions in the integral over x can be replaced by unity, and the Wigner surmise for the GSE follows trivially.

The distribution $P_{1 \to 4}(s; \lambda)$ is plotted for several values of λ in Fig. 2 (middle) and displays a continuous interpolation between the GOE and GSE curves. In the small-s region, the level repulsion is of fourth order for nonvanishing λ. This is visible in the plots and can be shown by expanding $P_{1 \to 4}(s; \lambda)$ for $\lambda > 0$ and small s,

$$
P_{1 \to 4}(s; \lambda) = c(\lambda) s^4 + O(s^6), \qquad (2.45)
$$

with

$$
c(\lambda) \sim \frac{\pi^2}{12\lambda^3} \quad \text{for } \lambda \to 0. \qquad (2.46)
$$

The large-s behavior of $P_{1 \to 4}(s; \lambda)$ can be obtained using the asymptotic expansion

$$
I_0(z) - I_1(z) = e^z \left[\frac{1}{\sqrt{8\pi}\, z^{3/2}} + O(z^{-5/2}) \right] \qquad (2.47)
$$

in Eq. (2.41), resulting in

$$
P_{1 \to 4}(s; \lambda) \sim \sqrt{\frac{\pi}{32}}\, \frac{C}{D^3}\, s\, e^{-2(\lambda D s)^2} \quad \text{for } s \to \infty. \qquad (2.48)
$$

Again, the large-s behavior is dominated by the ensemble with the smaller β.

G. GUE to GSE

Again, due to the presence of the GSE, we have two possibilities for the GUE: self-dual or not. The former case is simpler and analyzed here, while the latter case will be considered in Sec. II H. We first have to clarify how to obtain a self-dual 4×4 matrix whose eigenvalues have the same probability distribution as those of a 2×2 matrix from the GUE. In analogy to Sec. II F, one could try $H_2 \otimes \mathbb{1}_2$, but the resulting matrix is not self-dual. Instead, we consider the matrix

$$
H_2^4 = \begin{pmatrix} H_2 & 0 \\ 0 & H_2^T \end{pmatrix} \qquad (2.49)
$$

with H_2 given in Eq. (2.11). The eigenvalues of H_2^4 are obviously equal to those of H_2, but they are twofold degenerate.

Interchanging the second and third row and column of H_2^4, we obtain the matrix

$$H_2^{\text{sd}} = \begin{pmatrix} a & 0 & c_0 + ic_1 & 0 \\ 0 & a & 0 & c_0 - ic_1 \\ c_0 - ic_1 & 0 & b & 0 \\ 0 & c_0 + ic_1 & 0 & b \end{pmatrix}, \quad (2.50)$$

which is self-dual and has the same eigenvalues as H_2^4. A matrix of this form was already introduced in Ref. [29].

The proper self-dual matrix for the GUE to GSE transition is thus

$$H = H_2^{\text{sd}} + \lambda H_4, \quad (2.51)$$

with H_4 given in Eq. (2.21). The calculation of the corresponding spacing distribution proceeds in close analogy with the one presented in Appendix C 2, and we find the closed expression

$$P_{2\to 4}(s;\lambda) = Ce^{-(\lambda Ds)^2}[2(Ds)^2 - \sqrt{\pi}\, Ds\, e^{-(Ds)^2}\, \text{erfi}(Ds)], \quad (2.52)$$

with the imaginary error function $\text{erfi}(x) = -i\,\text{erf}(ix)$ and

$$D(\lambda) = \frac{1}{\lambda\sqrt{\pi}}\left(2 + \lambda^2 - \lambda^4\,\frac{\text{arccsch}\,\lambda}{\sqrt{1+\lambda^2}}\right), \quad (2.53)$$

$$C(\lambda) = \frac{2\lambda^3}{\sqrt{\pi}}(1 + \lambda^2)D(\lambda), \quad (2.54)$$

where arccsch is defined in Ref. [[35], Eq. (4.6.17)].

In the limiting cases of $\lambda \to 0$ and $\lambda \to \infty$ we have

$$D(\lambda) \sim \begin{cases} 2/(\lambda\sqrt{\pi}) & \text{for} \quad \lambda \to 0, \\ 8/(3\lambda\sqrt{\pi}) & \text{for} \quad \lambda \to \infty. \end{cases} \quad (2.55)$$

For $\lambda \to 0$, the asymptotic expansion of the second term in the square brackets of Eq. (2.52) yields -1. This can be neglected compared to the first term in the square brackets, which gives the Wigner surmise for the GUE. For $\lambda \to \infty$, Taylor expansion of the square brackets in Eq. (2.52) yields the Wigner surmise for the GSE.

The result (2.52) is plotted in Fig. 2 (right). In the small-s region, we have for $\lambda \neq 0$

$$P_{2\to 4}(s;\lambda) = c(\lambda)s^4 + O(s^6), \quad (2.56)$$

with

$$c(\lambda) \sim \frac{256}{3\pi^3\lambda^2} \quad \text{for} \quad \lambda \to 0. \quad (2.57)$$

The large-s behavior of $P_{2\to 4}(s;\lambda)$ can be obtained by noticing that for large s the first term in the square brackets of Eq. (2.52) dominates the second term so that

$$P_{2\to 4}(s;\lambda) \sim 2CD^2 s^2 e^{-(\lambda Ds)^2} \quad \text{for} \quad s \to \infty. \quad (2.58)$$

Again, the large-s behavior is dominated by the ensemble with the smaller β.

H. GSE to GUE without self-dual symmetry

In this section, we consider a matrix taken from the GSE whose Kramers degeneracy is lifted by a perturbation taken from the GUE without self-dual symmetry. As we shall see, this case also gives a surmise for other transitions involving
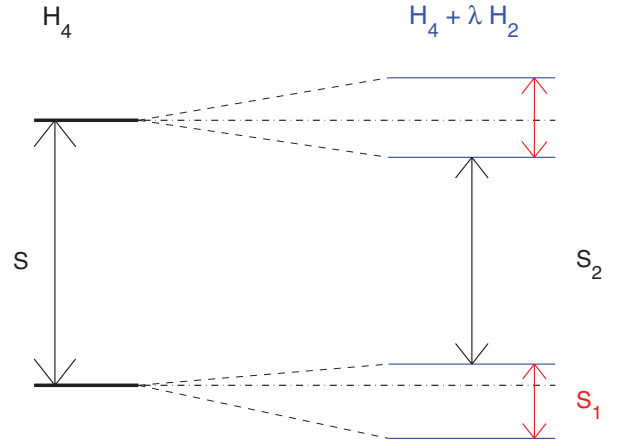

FIG. 3. (Color online) Perturbation of GSE eigenvalues removing the degeneracy.

the GSE and another ensemble without self-dual symmetry. We will return to this point in Sec. III E.

1. General considerations

The 4×4 transition matrix is

$$H = H_4 + \lambda H_2, \quad (2.59)$$

with H_4 taken from the GSE and H_2 from the GUE, both in standard normalization, Eq. (2.2). As H_2 has no self-dual symmetry, the twofold degeneracy of the GSE spectrum is removed and eigenvalue pairs are split up. If the perturbation is small, there are two different spacing scales in this setup, as shown in Fig. 3 where the perturbation of two nearest-neighbor eigenvalues is sketched:

S_1: the spacings between previously degenerate eigenvalues, which are of the same order of magnitude as the coupling parameter for small couplings; these are formed by the two smallest and the two largest eigenvalues of H;

S_2: the intermediate spacing, which is formed by the second and third largest eigenvalue of H; in the limit $\lambda \to 0$ this is the original spacing of the GSE matrix H_4.

The joint probability density of the eigenvalues of H is given, up to a rescaling, by [5, Eq. (14.2.7)]

$$P(\theta_1,\theta_2,\theta_3,\theta_4)$$
$$= C_0 \exp\left(-\sum_{i=1}^{4}\theta_i^2\right)\Delta(\theta_1,\theta_2,\theta_3,\theta_4)$$
$$\times [h(d_{21})h(d_{43}) + h(d_{32})h(d_{41}) - h(d_{31})h(d_{42})], \quad (2.60)$$

with

$$\Delta(\theta_1,\theta_2,\theta_3,\theta_4) = \prod_{i<j}(\theta_j - \theta_i), \quad (2.61)$$

$$h(x) = xe^{-x^2/\lambda^2}, \quad (2.62)$$

$$d_{ij} = \theta_i - \theta_j, \quad (2.63)$$

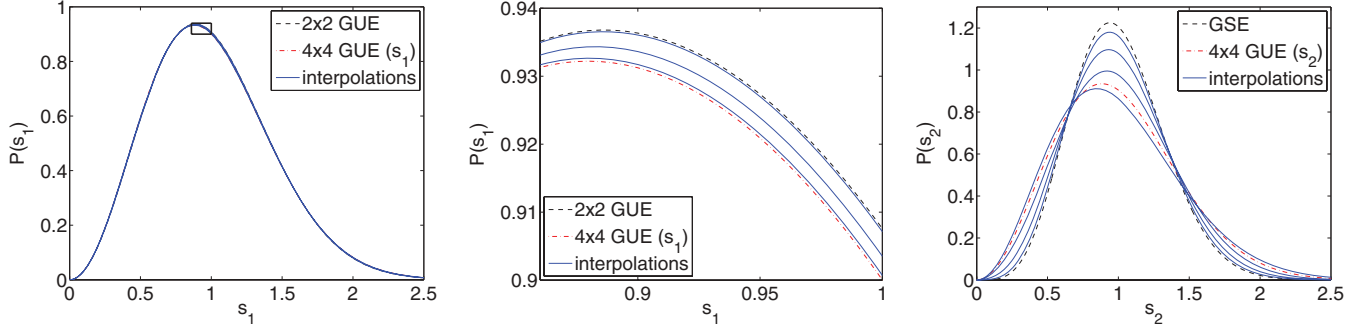$$C_0 = \frac{1}{9\pi^2}\lambda^{-6}(2+\lambda^2)^5. \quad (2.64)$$

FIG. 4. (Color online) Spacing distributions for the transition from GSE → GUE (non-self-dual) for 4×4 matrices and various values of the coupling parameter λ. Left: Spacings s_1 between previously degenerate eigenvalues. Middle: Spacings s_1, but zoomed in to the rectangular region indicated in the plot on the left; 2×2 GUE stands for $\lambda \to 0$; 4×4 GUE stands for $\lambda \to \infty$; for the interpolation curves we chose $\lambda = 0.4, 1, 2$ (maxima decreasing). Right: Intermediate spacing s_2; GSE stands for $\lambda = 0$; 4×4 GUE stands for $\lambda \to \infty$; for the interpolation curves we chose $\lambda = 0.05, 0.15, 0.3, 1$ (maxima decreasing).

As we are only interested in spacings and thus in differences of eigenvalues, we introduce new variables

$$t_1 = d_{21} = \theta_2 - \theta_1, \quad (2.65)$$
$$t_2 = d_{32} = \theta_3 - \theta_2, \quad (2.66)$$
$$t_3 = d_{43} = \theta_4 - \theta_3 \quad (2.67)$$

and keep the original variable θ_1. The Jacobi determinant of this transformation is 1, and we can now perform the θ_1 integration, which results (up to a constant factor) in

$$
\begin{aligned}
P(t_1, t_2, t_3) = {} & \Delta(-t_1, 0, t_2, t_2 + t_3) \\
& \times \exp\left\{ -\tfrac{1}{4} \left[(t_1 + 2t_2 + t_3)^2 + 2t_1^2 + 2t_3^2 \right] \right\} \\
& \times \left[h(t_1) h(t_3) - h(t_1 + t_2) h(t_2 + t_3) \right. \\
& \left. + h(t_1 + t_2 + t_3) h(t_2) \right].
\end{aligned}
\quad (2.68)
$$

We now derive the distributions of the two different kinds of spacings from this formula. We assume $\theta_1 \leqslant \theta_2 \leqslant \theta_3 \leqslant \theta_4$ and include the resulting combinatorial factor of 4! explicitly.

2. Spacings between originally degenerate eigenvalues

To obtain the distribution of the spacing between the two smallest eigenvalues of H (the two largest ones give the same result due to symmetry), we set $t_1 = S_1$ and integrate over t_2 and t_3 from 0 to ∞. This results in the spacing distribution

$$P_{4 \to 2}^1(s_1; \lambda) = C D \int_0^\infty dt_2 \, dt_3 \, P(Ds_1, t_2, t_3), \quad (2.69)$$

with

$$C(\lambda) = \frac{4}{3} \pi^{-3/2} \lambda^{-6} (2 + \lambda^2)^5, \quad (2.70)$$

$$D(\lambda) = C(\lambda) \int_0^\infty dS_1 \, dt_2 \, dt_3 \, S_1 \, P(S_1, t_2, t_3). \quad (2.71)$$

We replaced S_1 by s_1 to indicate that this is the spacing on the unfolded scale, i.e., with a mean value of 1. One of the integrals could in principle be done analytically, but this results in such a lengthy expression that it seems more sensible to evaluate all integrals numerically.

The distribution in the limit $\lambda \to 0$ can either be obtained by perturbation theory (see Appendix D 1) or by directly

evaluating the spacing distribution in the limit $\lambda \to 0$. First note that

$$\lim_{\lambda \to 0} \frac{2}{\sqrt{\pi} \lambda^3} \, x \, h(x) = \delta(x), \quad (2.72)$$

where the λ dependence of h, which is suppressed in our notation, plays a crucial role. As the mean value of the spacing S_1 on the original scale has to become arbitrarily small in the GSE limit due to the Kramers degeneracy, we consider a rescaled spacing $\tilde{s}_1 = S_1 / \lambda$. Therefore $h(S_1)$ becomes for small λ

$$h(S_1) = h(\lambda \tilde{s}_1) \overset{\lambda \to 0}{\approx} \lambda \tilde{s}_1 \, e^{-\tilde{s}_1^2}. \quad (2.73)$$

With these considerations we obtain from Eq. (2.68)

$$
\begin{aligned}
P(\lambda \tilde{s}_1, {} & t_2, t_3) \\
& \propto \lambda \, e^{-\frac{1}{4}[(\lambda \tilde{s}_1 + 2t_2 + t_3)^2 + 2\lambda^2 \tilde{s}_1^2 + 2t_3^2]} \\
& \times \left[\frac{2\tilde{s}_1^2}{\sqrt{\pi} \lambda} e^{-\tilde{s}_1^2} \delta(t_3)(\lambda \tilde{s}_1 + t_2)(\lambda \tilde{s}_1 + t_2 + t_3) t_2 (t_2 + t_3) \right. \\
& \quad - \delta(\lambda \tilde{s}_1 + t_2) \, \delta(t_2 + t_3) \lambda \tilde{s}_1 t_2 t_3 (\lambda \tilde{s}_1 + t_2 + t_3) \\
& \quad \left. + \delta(\lambda \tilde{s}_1 + t_2 + t_3) \, \delta(t_2) \lambda \tilde{s}_1 (\lambda \tilde{s}_1 + t_2)(t_2 + t_3) t_3 \right] \quad (2.74)
\end{aligned}
$$

as $\lambda \to 0$. The last two terms in square brackets vanish upon evaluation of the t_2 and t_3 integrals, because the zeros of the arguments of their δ functions lie outside of the integration region. Performing the t_3 integration in the first term we obtain for nonzero λ and $\tilde{s}_1$

$$P_{4 \to 2}^1(\tilde{s}_1; \lambda) \overset{\lambda \to 0}{\propto} \tilde{s}_1^2 \, e^{-\tilde{s}_1^2}. \quad (2.75)$$

Up to normalization and rescaling this is the spacing distribution of a 2×2 GUE matrix.

In the opposite limit $\lambda \to \infty$ the result (2.69) reduces to the distribution of the first and last spacings of a pure 4×4 GUE matrix. This distribution can be obtained from similar considerations, starting from [5, Eq. (3.3.7)].

The result (2.69) is shown in Fig. 4 (left and middle) for several values of λ, along with the limiting distributions for $\lambda \to 0$ and $\lambda \to \infty$. All these curves are very similar and can only be distinguished by the naked eye in the zoomed-in plot.

We have validated the result (2.69) by comparing it to the spacing distribution of numerically obtained 4×4 random matrices.

3. Perturbed GSE spacing

We now consider the perturbed spacing of the original GSE matrix, which was formed by the two degenerate eigenvalue pairs of H_4. The distribution of this spacing is obtained by setting $t_2 = S_2$ and integrating P defined in Eq. (2.68) over t_1 and t_3 from 0 to ∞. With proper normalization as given in Eq. (2.2), this yields

$$P_{4\to2}^2(s_2; \lambda) = C D \int_0^\infty dt_1 \, dt_3 \, P(t_1, Ds_2, t_3), \quad (2.76)$$

with

$$C(\lambda) = \frac{4}{3} \pi^{-3/2} \lambda^{-6} (2 + \lambda^2)^5, \quad (2.77)$$

$$D(\lambda) = C(\lambda) \int_0^\infty dS_2 \, dt_1 \, dt_3 \, S_2 \, P(t_1, S_2, t_3). \quad (2.78)$$

Again, the replacement of S_2 by s_2 means that this is the intermediate spacing on the unfolded scale, i.e., with a mean value of 1.

In the limit $\lambda \to 0$ the result (2.76) reduces to the Wigner surmise for the GSE, while in the opposite limit $\lambda \to \infty$ it reduces to the spacing distribution of the intermediate spacing of a pure 4×4 GUE matrix, which can again be obtained from similar considerations.

The result (2.76) is shown in Fig. 4 (right) for several values of λ, along with the limiting distributions for $\lambda \to 0$ and $\lambda \to \infty$. The maximum of the interpolation first drops down as λ is increased from 0, while at a value of λ around 1 it starts to rise again as the distribution approaches its $\lambda \to \infty$ limit. Note that the limiting distributions of s_1 and s_2 for $\lambda \to \infty$, i.e., the red dashed curves in Fig. 4, turn out to be almost identical to each other and to the Wigner surmise for the GUE.

We have also validated the result (2.76) by comparing it to the spacing distribution of numerically obtained 4×4 random matrices.

III. APPLICATION TO LARGE SPECTRA

In this section we will show numerically that the formulas derived in Sec. II for small matrices describe the spacing distributions of large random matrices very well. This observation should be viewed as our main result.

When comparing the results obtained from large matrices to our generalized Wigner surmises, a natural question is how the corresponding coupling parameters, i.e., λ in Eq. (1.4), should be matched. This question will be addressed in the next section based on perturbation theory, while the numerical results will be presented in the remaining portions of Sec. III.

A. Matching of the coupling parameters

The setup is most easily explained by means of the transition from Poisson to the GUE. The Poisson case is represented by a diagonal $N \times N$ matrix H_0 with independent entries θ_i ($i = 1, \dots, N$), each distributed according to the same distribution $\mathcal{P}(\theta)$, which we choose independent of N. The eigenvalue density of H_0 is thus $\rho_0(\theta) = N \mathcal{P}(\theta)$, and the local mean level spacing is $1/\rho_0(\theta)$. We consider

$$H = H_0 + \alpha H_2, \quad (3.1)$$

where H_2 is an $N \times N$ random matrix taken from the GUE, subject to the usual normalization, Eq. (2.2).

As in the 2×2 case, the eigenvalues θ_i will experience a repulsion through H_2. We will show in first-order perturbation theory that the relevant quantity for the repulsion is a combination of the eigenvalue density of H_0 and the variance of the matrix elements of H_2.

Ordinary perturbation theory in α yields a first-order eigenvalue shift of the θ_i of

$$\Delta \theta_i^{(1)} = \alpha (H_2)_{ii}. \quad (3.2)$$

This shift does not lead to a correlation of the eigenvalues, as it just adds an independent Gaussian random number to each of them. Therefore, the eigenvalues remain uncorrelated, and their spacing distribution remains Poissonian.

However, if there is a small spacing of order α between two[5] adjacent eigenvalues θ_k and θ_ℓ of H_0, first-order almost-degenerate perturbation theory [40] predicts that the perturbed eigenvalues are the eigenvalues of the matrix

$$\begin{pmatrix} \theta_k & 0 \\ 0 & \theta_\ell \end{pmatrix} + \alpha \begin{pmatrix} (H_2)_{kk} & (H_2)_{k\ell} \\ (H_2)_{\ell k} & (H_2)_{\ell\ell} \end{pmatrix}. \quad (3.3)$$

This matrix is almost identical to the 2×2 matrix considered in Sec. II C, Eq. (2.11), with two differences: (i) The unperturbed eigenvalues θ_k and θ_l are shifted, but this does not affect the spacing distribution. (ii) The mean spacing of the unperturbed eigenvalues is not 1, but $1/\rho_0(\theta)$. We dropped the subscript on the eigenvalue θ here, because adjacent eigenvalues are very close for large N, and therefore $\rho_0(\theta_k) \approx \rho_0(\theta_\ell) = \rho_0(\theta)$.

To be able to match to the 2×2 formulas, we have to correct for the different mean spacing of the unperturbed matrix. We can do this by multiplying the matrix in Eq. (3.3) by $\rho_0(\theta)$ without affecting the normalized spacing distribution. This results in the relation

$$\lambda(\theta) = \rho_0(\theta) \alpha \quad (3.4)$$

between the coupling parameters of the 2×2 case and the $N \times N$ cases. Note that the 2×2 parameter λ has acquired a dependence on the eigenvalue θ of H through the local eigenvalue density of H_0. To be able to describe the spacing distribution of H in the spectral region around θ by the generalized Wigner surmise, we assume that we have to insert this $\lambda(\theta)$ into the 2×2 formulas. This choice of universal coupling parameter is in line with an "unfolded" coupling parameter mentioned in Refs. [32,41] and a similar result from perturbation theory [42]. Appendix E contains a calculation for large matrices in second-order perturbation theory, also showing that the strength of the perturbation to be used in the generalized Wigner surmise only depends on the combination $\rho_0(\theta) \alpha$.

---

[5]For small α, we are unlikely to find three or more small (i.e., of order α) consecutive spacings.

We now turn from the example "Poisson to GUE" to the general case, which we write as

$$H = H_\beta + \alpha H_{\beta'}. \tag{3.5}$$

The same considerations hold with two modifications: (i) The unperturbed matrix is not necessarily diagonal by construction. However, it can be diagonalized by a transformation that can be absorbed in the perturbation.[6] We can therefore treat it as diagonal (with eigenvalues correlated as dictated by the unperturbed ensemble). (ii) The mean spacing $\bar{s}_\beta$ of the unperturbed 2×2 (4×4) matrix from Sec. II is

$$\bar{s}_0 = 1 (\text{Poisson}), \quad \bar{s}_1 = \sqrt{\pi} (\text{GOE}),$$
$$\bar{s}_2 = \frac{4}{\sqrt{\pi}} (\text{GUE}), \quad \bar{s}_4 = \frac{16}{3\sqrt{\pi}} (\text{GSE}). \tag{3.6}$$

Therefore, we now have to multiply Eq. (3.5) by $\bar{s}_\beta \rho_\beta(\theta)$ to get the correct mean spacing $\bar{s}_\beta$ for the unperturbed matrix. This results in a universal, but θ-dependent, coupling parameter

$$\lambda(\theta) = \bar{s}_\beta \rho_\beta(\theta) \alpha \tag{3.7}$$

with the eigenvalue density $\rho_\beta(\theta)$ of the unperturbed matrix. Equation (3.7) holds for all the transitions we consider, and in each case β is the Dyson index of the unperturbed ensemble.

In turn, this perturbative argument provides us with a formula of how to choose the coupling α in large matrices in order to approximate the spacing distribution of H by 2×2 (4×4) formulas with parameter λ, i.e.,

$$\alpha = \frac{\lambda}{\rho_\beta(\theta) \bar{s}_\beta}, \tag{3.8}$$

where $\rho_\beta(\theta)$ is the eigenvalue density in the spectral region we wish to study. In this way we can choose a value of λ resulting in a spacing distribution roughly in the middle of the two limiting cases. Choosing α in Eq. (3.5) without this guidance is likely to result in a spacing distribution that is dominated by one of the limiting cases.

B. Transitions from integrable to chaotic

1. Check of Wigner surmise

We first consider transitions from Poisson to RMT for matrices with N nondegenerate eigenvalues. The explicit numerical realization is the Hamiltonian

$$H = H_0 + \frac{\Lambda}{\rho_0(0)} H_{\beta'}, \tag{3.9}$$

where $H_{\beta'}$ is a matrix taken from one of the Gaussian ensembles, with normalization as given in Eq. (2.2). H_0 is the same matrix as in Eq. (3.1) for the perturbation $H_{\beta'}$ in GOE or GUE, whereas a self-dual H_0 is constructed by a direct product with $\mathbb{1}_2$ as in Sec. II D if the perturbation is

_____

[6]Note that we choose the perturbations $H_{\beta'}$ such that their probability distribution is always invariant under the transformations that diagonalize H_β, just like in the Poisson to RMT cases. However, this does not work for some of the transitions between the GSE and ensembles without self-dual symmetry, which we discuss separately in Sec. III E.

taken from the GSE. We choose a Gaussian for the distribution of the eigenvalues of H_0, i.e., $\mathcal{P}(\theta) = (1/\sqrt{2\pi}) \exp(-\theta^2/2)$, so $\rho_0(0) = N/\sqrt{2\pi}$. From Eq. (3.8) we would then expect the spacing distribution in the center of the spectrum around $\theta = 0$ to be approximated by the corresponding 2×2 formulas (2.4), (2.12), and (2.26) with coupling $\lambda = \Lambda$.

As can be seen in Fig. 5, the formulas for the 2×2 matrices indeed describe the spectra of large matrices quite well in a wide range of the coupling parameter Λ. The spacing distribution was evaluated in the center of the spectrum, defined as the interval $(-0.2, 0.2)$, because the eigenvalue density is almost constant and equal to $\rho_0(0)$ in this region so that no unfolding is needed. The analytical curve was obtained by a fit (see Appendix F for details) of the 2×2 (or 4×4) formula to the numerical data with fit parameter λ. As expected by the perturbative considerations, λ comes out on the same order of magnitude as Λ, and it almost matches for small Λ. However, λ is considerably smaller than Λ for stronger couplings. Presumably, the repulsion of the many other eigenvalues in the spectrum not present in the smallest matrices has a squeezing effect on the spacing, which works against the repulsion caused by the perturbation. This would explain the smaller coupling parameter.

2. Dependence of coupling parameter on eigenvalue density

The considerations in Sec. III A imply a linear relation between local eigenvalue density and effective coupling parameter, Eq. (3.7), for matrices of the form given in Eq. (3.1). This means that a perturbation should have a different impact on the spacing distribution of a single matrix in different regions of its spectrum (as qualitatively observed in Ref. [15]). This section provides a detailed analysis of this phenomenon.

Again, we consider a diagonal Poissonian matrix H_0 of large dimension perturbed by a matrix taken from one of the Gaussian ensembles $H_{\beta'}$,

$$H = H_0 + \alpha H_{\beta'}. \tag{3.10}$$

This time we will choose some fixed α and look separately at different parts of the spectrum of H with a varying eigenvalue density. According to Eq. (3.7) the effective 2×2 (4×4) coupling parameter λ should be the product of α and the local eigenvalue density of H_0. In Appendix E we show in perturbation theory up to second order that the local coupling parameter is in fact a function of this product.

To treat such a system numerically one has to construct a Poissonian ensemble with a varying eigenvalue density, perturb it, and measure the coupling parameter in different parts of the spectrum. This is done by cutting the spectrum into small windows with approximately constant eigenvalue density and fitting (see Appendix F for details) the spacing distributions inside the windows to the formulas for the 2×2 (4×4) matrices. We therefore obtain a fitted coupling parameter λ for each window.

For the numerical calculations, the eigenvalues θ_i of the matrix H_0 were distributed in the interval $(-N/2, N/2)$ according to the somewhat arbitrarily chosen distribution

$$\mathcal{P}(\theta_i) = \frac{1}{N} \left[\frac{1}{2} + 6 \left(\frac{\theta_i}{N} \right)^2 + 8 \left(\frac{\theta_i}{N} \right)^3 \right], \tag{3.11}$$
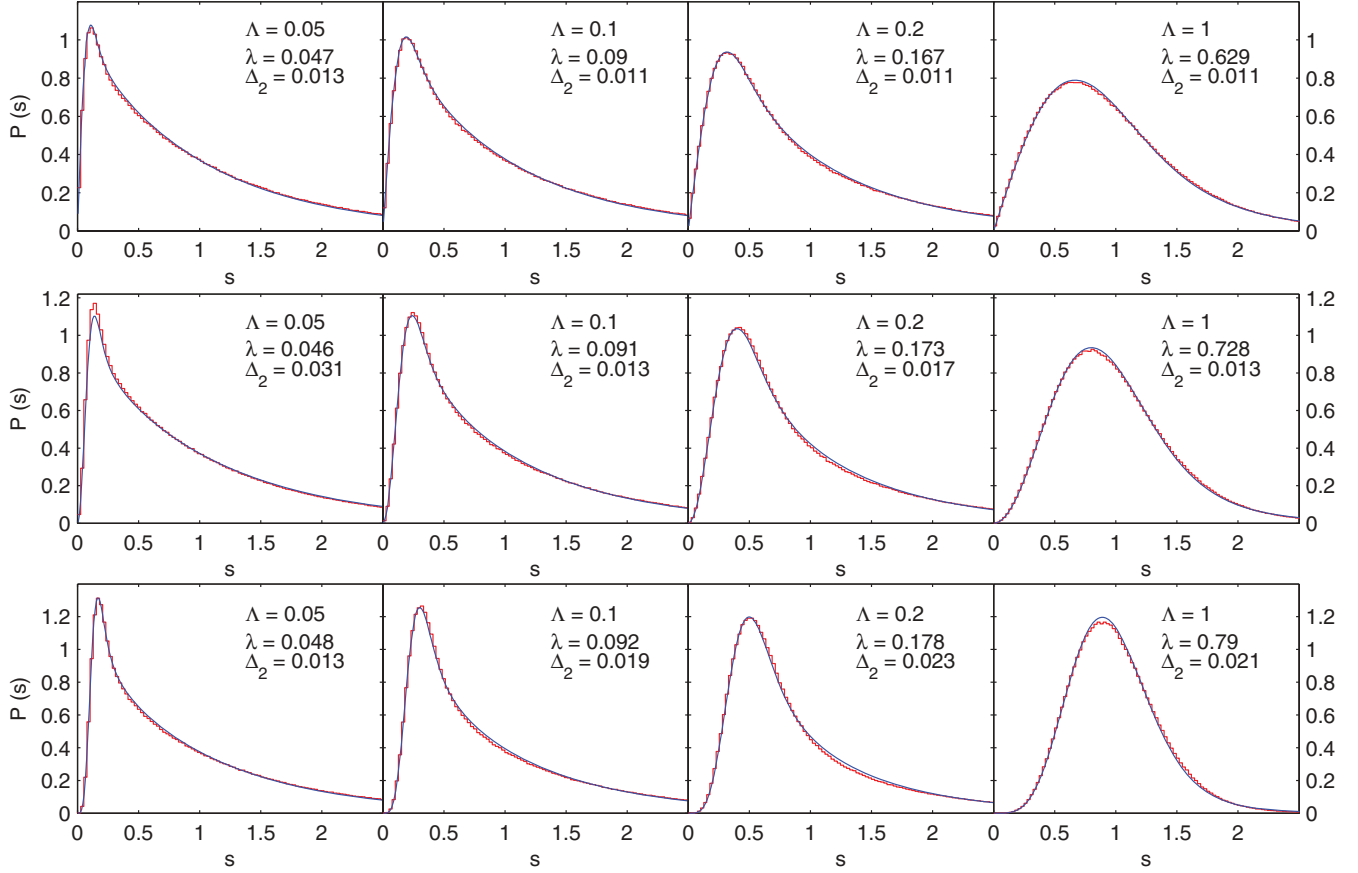
FIG. 5. (Color online) Spacing distributions for the transition of large matrices from Poisson to GOE (top), GUE (middle), and GSE (bottom) with several values of the coupling Λ in Eq. (3.9). The histograms show the numerical data, while the full curves are the analytical results for 2×2 (4×4) matrices with fitted coupling parameter λ; see Secs. II B through II D. The quantity Δ_2 defined in Appendix F is a measure of the fit quality, which is small for a good fit. Each plot has been obtained by diagonalizing 50 000 matrices with 400 nondegenerate eigenvalues.

N being the number of independent eigenvalues of H_0. The matrix $H_{\beta'}$ is normalized in the usual way, Eq. (2.2).

The eigenvalue density $\rho(\theta)$ of the total matrix H is plotted along with the analytical $\rho_0(\theta) = N\mathcal{P}(\theta)$ of H_0 in the top row of Fig. 6. One can see that the perturbation only has a negligible effect on the spectral density.

The dependence of the coupling parameter on the eigenvalue density is plotted in the bottom row of Fig. 6 for $\alpha = 0.1$. No error bars are shown because the statistical errors are negligibly small. A linear fit through the origin with minimized squared deviation was performed to obtain the proportionality factor between the eigenvalue density and the coupling parameter. The quantity δ_2 shown in the plots is a measure of the fit quality and defined by

$$\delta_2 = \sqrt{\sum_{i=1}^{N} \frac{(\lambda_i - \tilde{\lambda}_i)^2}{N} \Big/ \sum_{j=1}^{N} \frac{\lambda_j}{N}}, \qquad (3.12)$$

where the λ_i are the numerically obtained coupling parameters for each spectral window and the $\tilde{\lambda}_i$ are the corresponding predictions from the linear fit at the given eigenvalue density. Because δ_2 is a monotonically increasing function of the squared deviation it is also minimized by our fitting procedure.

As can be seen, the linear dependence of the effective coupling parameter on the eigenvalue density is confirmed very well by the numerical data for all the transitions. Note that the fit quality gets better with increasing Dyson index β'; i.e., it is worst for the GOE and best for the GSE. This is most likely explained by the fact that the spacing distributions change more rapidly with respect to the coupling parameter for larger β' (cf. Fig. 1), which allows for a more precise measurement of the coupling.

Although the linear dependence of the effective coupling on the eigenvalue density has been demonstrated beyond reasonable doubt, the proportionality factor is less clear. As can be read off from Fig. 6 the proportionality factor is smaller than α; i.e., the measured coupling parameter is smaller than the expected one. This agrees with the observation in Sec. III B 1 where an explanation was given in terms of the effect of other eigenvalues.

C. Transitions from one symmetry class to another

1. Check of Wigner surmise

We now consider chaotic systems composed of different symmetry classes, the latter represented by pure Gaussian
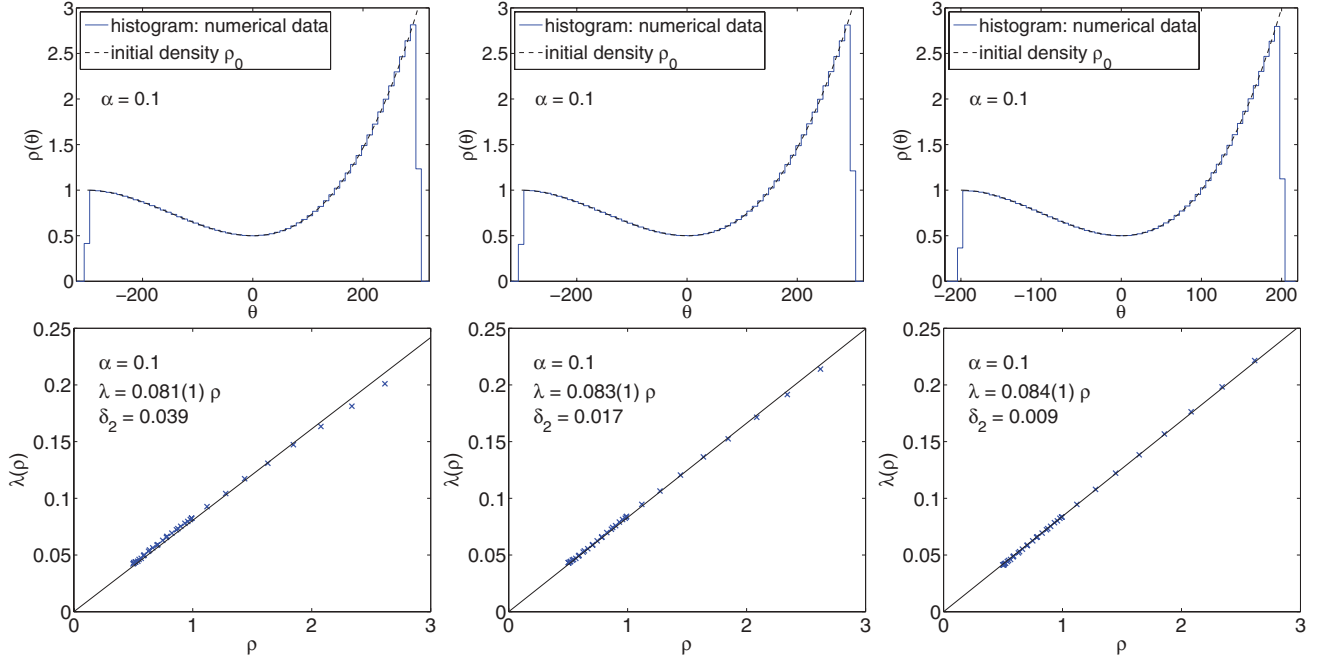
FIG. 6. (Color online) Transitions Poisson $\to$ GOE (left), Poisson $\to$ GUE (middle), and Poisson $\to$ GSE (right). Top: Unperturbed and perturbed eigenvalue density, the latter obtained numerically. Bottom: Effective coupling λ obtained from fits of the 2×2 (4×4) level spacings $P_{0 \to \beta'}(s)$ [see Eqs. (2.4), (2.12), and (2.26)] as a function of the local eigenvalue density in 35 equally large windows of the spectrum. Linear fit and proportionality factor with errors defined by the 95% confidence interval are given in the plots. The quantity δ_2 defined in Eq. (3.12) is a measure of the fit quality, which is small for a good fit. The numerical data were obtained from 10^5 random matrices of dimension 600 (GOE and GUE) or 800 (GSE).

ensembles. If the GSE is involved, we consider the case of a self-dual perturbed ensemble in this section (see Sec. III D for the case of a non-self-dual perturbed ensemble). A self-dual GOE can be constructed by taking the direct product with $\mathbb{1}_2$ as in Sec. II F, while the self-dual GUE is more involved (see Appendix G). All ensembles are normalized as in Eq. (2.2). Again motivated by Eq. (3.8), we consider the Hamiltonian

$$H = H_\beta + \frac{\Lambda}{\rho_\beta(0)\bar{s}_\beta} H_{\beta'}. \qquad (3.13)$$

For large matrix size, the eigenvalue density of H_β is a semicircle which extends to $r_\beta = \sqrt{2\beta N}$, and its eigenvalue density in the center is

$$\rho_\beta(0) = \frac{\sqrt{2N}}{\sqrt{\beta}\pi}. \qquad (3.14)$$

The results for the three transitions among the Gaussian ensembles are shown in Fig. 7 for $N = 400$. Again, only the center of the spectrum, defined as the interval $(-5, 5)$, was evaluated. (The whole semicircle extends to about ± 28 for $H_\beta \in$ GOE and about ± 40 for $H_\beta \in$ GUE.) The coupling parameter λ was obtained by a fit (see Appendix F for details) to the corresponding 2×2 (4×4) formula, which yields a good approximation to the numerical data throughout the transition in each case. As in Sec. III B 1, λ is close to Λ as expected.

For $\Lambda = 1$ and $N = 400$ the mixed matrix is roughly given by $H = H_\beta + O(10^{-1})H_{\beta'}$. From the λ values given in Fig. 7, which should be compared to those in Fig. 2, we see that

the transition is almost completed in this case and that the spacing distribution is already very similar to the one of the perturbing ensemble. What is relevant for the transition is not the relative magnitude of the matrix elements (which depends on N through the local eigenvalue density) but the rescaled coupling parameter Λ; i.e., the transition occurs for $\Lambda = O(1)$. The same phenomenon was found for the two-point function [41], which is related to the spacing distribution for small s.

2. Dependence of coupling parameter on eigenvalue density

We now consider the dependence of the coupling parameter on the local eigenvalue density as in Sec. III B 2, but now for transitions between Gaussian ensembles. In these cases, the fitting procedure of the effective coupling becomes less precise, because the functions of the spacing distributions change only very slowly with λ, as can be seen in Fig. 2. Therefore, we restrict ourselves to the case of a self-dual GOE matrix H_1 that is perturbed by a GSE matrix H_4 as the level repulsion differs the most in these two ensembles.

In Fig. 8 we show results from the mixed matrix

$$H = H_1 + \alpha H_4, \quad \alpha = \frac{\gamma}{\rho_1(0)\bar{s}_1}, \qquad (3.15)$$

with $\gamma = 0.2$. (For details about the self-dual GOE and the normalization, see Sec. III C 1.) According to Eq. (3.8) the effective 4×4 coupling parameter λ should be $\alpha\rho(\theta)\bar{s}_1 = \gamma\rho(\theta)/\rho_1(0)$, i.e., proportional to the local eigenvalue density
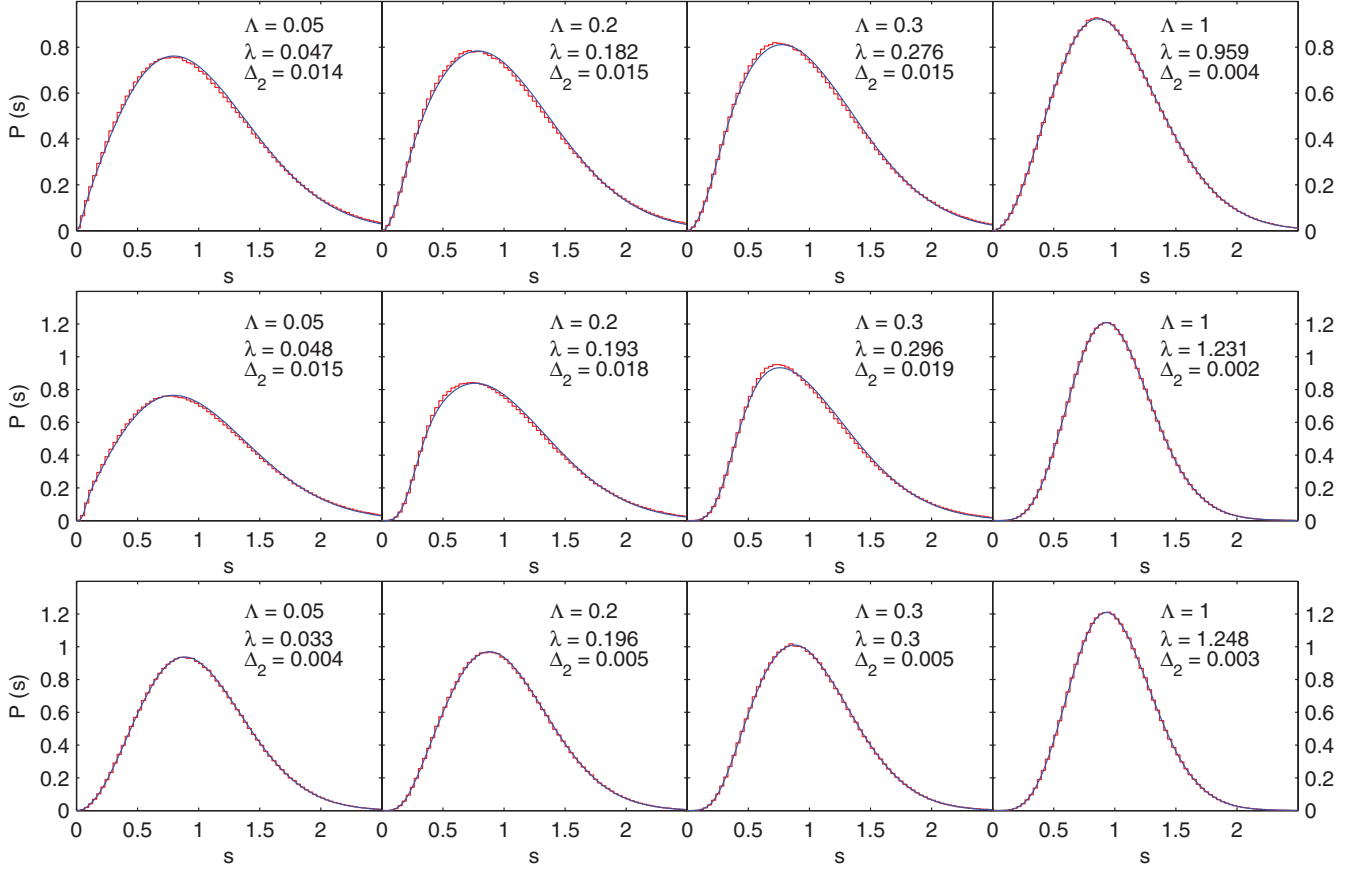
FIG. 7. (Color online) Spacing distributions for the transition of large matrices: GOE $\rightarrow$ GUE (top), GOE $\rightarrow$ GSE (middle), and GUE $\rightarrow$ GSE (bottom), with several values of the coupling Λ in Eq. (3.13). The histograms show the numerical data, while the full curves are the analytical results for 2×2 (4×4) matrices with fitted coupling parameter λ (see Secs. II E through II G). The quantity Δ_2 defined in Appendix F is a measure of the fit quality, which is small for a good fit. Each plot has been obtained by diagonalizing 50 000 matrices with 400 nondegenerate eigenvalues.

normalized by the density $\rho_1(0)$ in the center, with the proportionality factor given by the input parameter γ. As one can see, there is again a linear dependence of the fitted coupling
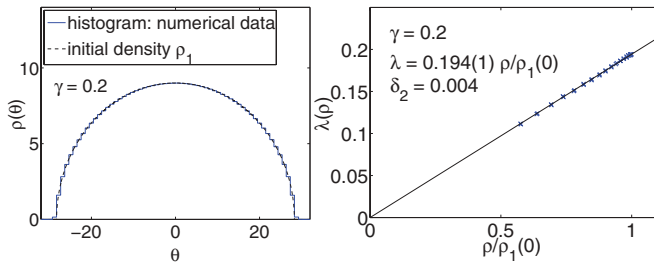

FIG. 8. (Color online) Transition GOE $\rightarrow$ GSE. Left: Unperturbed eigenvalue density (approximated by a semicircle) and perturbed eigenvalue density. Right: Effective coupling λ obtained from fits of the 4×4 level spacings $P_{1\rightarrow4}(s)$ [see Eq. (2.41)], as a function of the local eigenvalue density in 35 equally large windows in the spectrum. Linear fit and proportionality factor with errors defined by the 95% confidence interval are given in the plots. The quantity δ_2 defined in Eq. (3.12) is a measure of the fit quality, which is small for a good fit. The numerical data were obtained from 10^5 random matrices of dimension 800.

parameter Λ on the local density (and again, the perturbation has no measurable effect on the eigenvalue density). The proportionality factor is almost compatible with the expected value γ.

D. Perturbation of a GSE matrix by a non-self-dual GUE matrix

In this section, we apply the formulas derived in Sec. II H for the spacing distributions of a 4×4 matrix from the GSE perturbed by a matrix from the GUE, this time without self-dual symmetry, to large matrices. We consider a $2N \times 2N$ matrix

$$H = H_4 + \frac{\Lambda}{\rho_4(0)\bar{s}_4} H_2, \qquad (3.16)$$

where H_4 is taken from the GSE and H_2 is the perturbation from the GUE. Both H_4 and H_2 are normalized in the usual way [see Eq. (2.2), and for the prefactor of H_2 see Sec. III A]. To ensure a constant eigenvalue density, we again restrict the measurements to the center of the spectrum, defined by the interval $(-5, 5)$. The numerically obtained spacing distributions were rescaled to a mean value of 1.
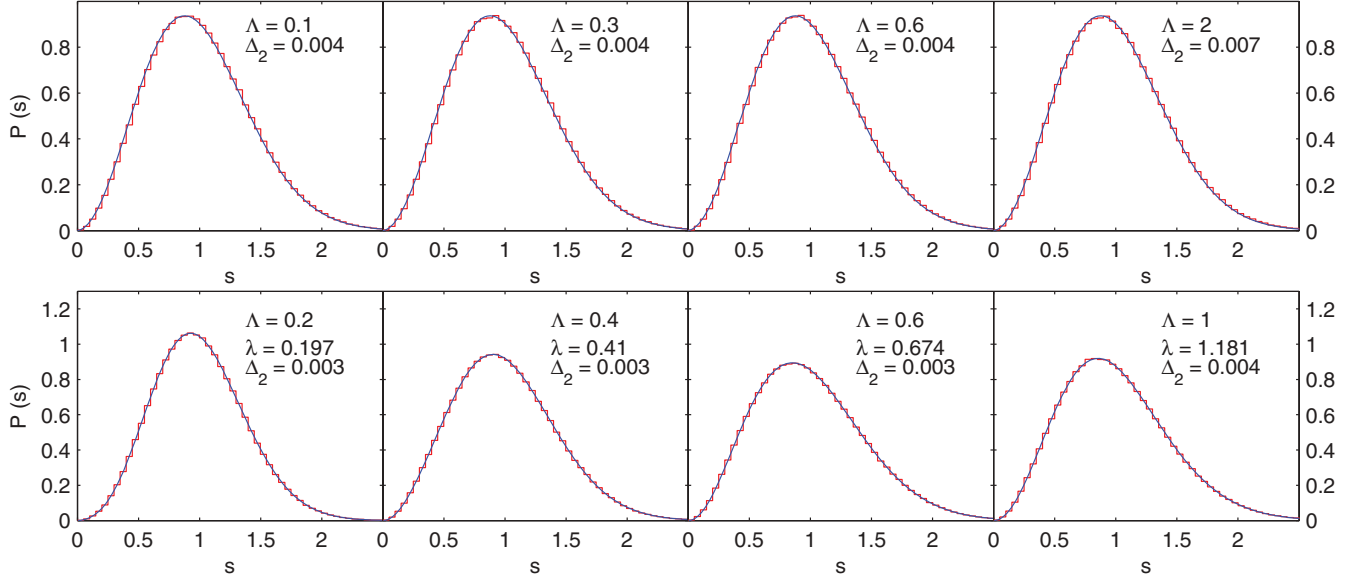
FIG. 9. (Color online) Spacing distributions between previously degenerate eigenvalues s_1 (top) and previously nondegenerate eigenvalues s_2 (bottom) for the transition GSE $\rightarrow$ GUE without self-dual symmetry for various values of the coupling parameter Λ in Eq. (3.16). The histograms show the numerical data, while the full curves are the 2×2 GUE surmise P_2 (top) and the surmise $P_{4\rightarrow2}^2(s_2;\lambda)$ given in Eq. (2.76) (bottom), the latter with fitted coupling parameter λ. The quantity Δ_2 defined in Appendix F is a measure of the fit quality, which is small for a good fit. The numerical data were obtained by diagonalizing 50 000 random matrices of dimension 400 for each plot.

As in Sec. II H, we will separately consider the spacings between originally degenerate eigenvalues and the remaining ones. The distributions of the former were obtained by measuring every second spacing, starting with the first one of each random matrix. They are plotted in Fig. 9 (top) and show perfect agreement with the 2×2 GUE surmise, which is practically indistinguishable from the exact result derived for 4×4 matrices, $P_{4\rightarrow2}^1(s_1;\lambda)$ given in Eq. (2.69). As in Sec. II H 2, this distribution is almost independent of the coupling parameter.

The distribution of the spacings between previously nondegenerate eigenvalues is shown in Fig. 9 (bottom). Again, every second spacing was measured, but starting with the second one this time. We get an almost perfect agreement of the numerical data with the surmise $P_{4\rightarrow\beta'}^2(s_2;\lambda)$ defined in Eq. (2.76) throughout the transition. The parameter λ was again determined by a fit (see Appendix F) and approximately matches the perturbative prediction from Sec. III A.

E. Other transitions between the GSE and ensembles without self-dual symmetry

Let us now consider the transition from the GSE to either the GOE or Poisson, both without self-dual symmetry. These two cases are more complicated than the cases discussed so far because, as we shall discuss now, the transitions proceed via an intermediate transition to the GUE.

Let us first focus on the case

$$H = H_4 + \frac{\Lambda}{\rho_4(0)\bar{s}_4} H_1, \qquad (3.17)$$

where H_4 is from the GSE, H_1 is from the GOE without self-dual symmetry, and we again concentrate on the central part of

the spectrum (near zero). For small Λ, we show in Appendix A in first-order perturbation theory that the perturbation by the GOE has exactly the same effect on the eigenvalues as the perturbation by the GUE considered in Sec. II H, modulo a rescaling of the coupling parameter, i.e.,

$$P_{4\rightarrow1}^1(s_1;\lambda) = P_{4\rightarrow2}^1(s_1;\lambda/\sqrt{2}) \simeq P_2(s_1), \qquad (3.18)$$

$$P_{4\rightarrow1}^2(s_2;\lambda) = P_{4\rightarrow2}^2(s_2;\lambda/\sqrt{2}). \qquad (3.19)$$

Therefore, we first expect a transition from the GSE to the GUE, corresponding to the breaking of the self-dual symmetry. This expectation is confirmed in Fig. 10 (top and middle).

As Λ is increased to very large values, a transition to GOE behavior must eventually occur. The question is whether this transition is described by the surmise of Sec. II E. We show in Fig. 10 (bottom) that this is indeed the case. Note that a rising Λ amounts to a shrinking fitted coupling parameter λ because the direction of the transition is turned around compared to Sec. II E. Here, $\Lambda \rightarrow \infty$ means that H is a pure GOE matrix, which is described by the surmise with $\lambda = 0$.

The case of GSE to Poisson without self-dual symmetry is analogous. For small values of the coupling parameter, the self-dual symmetry of the GSE is broken by the perturbation so that we expect a GSE to GUE transition for the spacings s_1 and s_2 as in the GSE to GOE case considered above. For very large values of the coupling parameter we should eventually find a transition to Poisson behavior, described by the surmise of Sec. II C. We have confirmed these expectations numerically but do not show the corresponding plots here.

Note that in the transitions considered in Secs. III B through III D a single antiunitary symmetry (or integrability in the
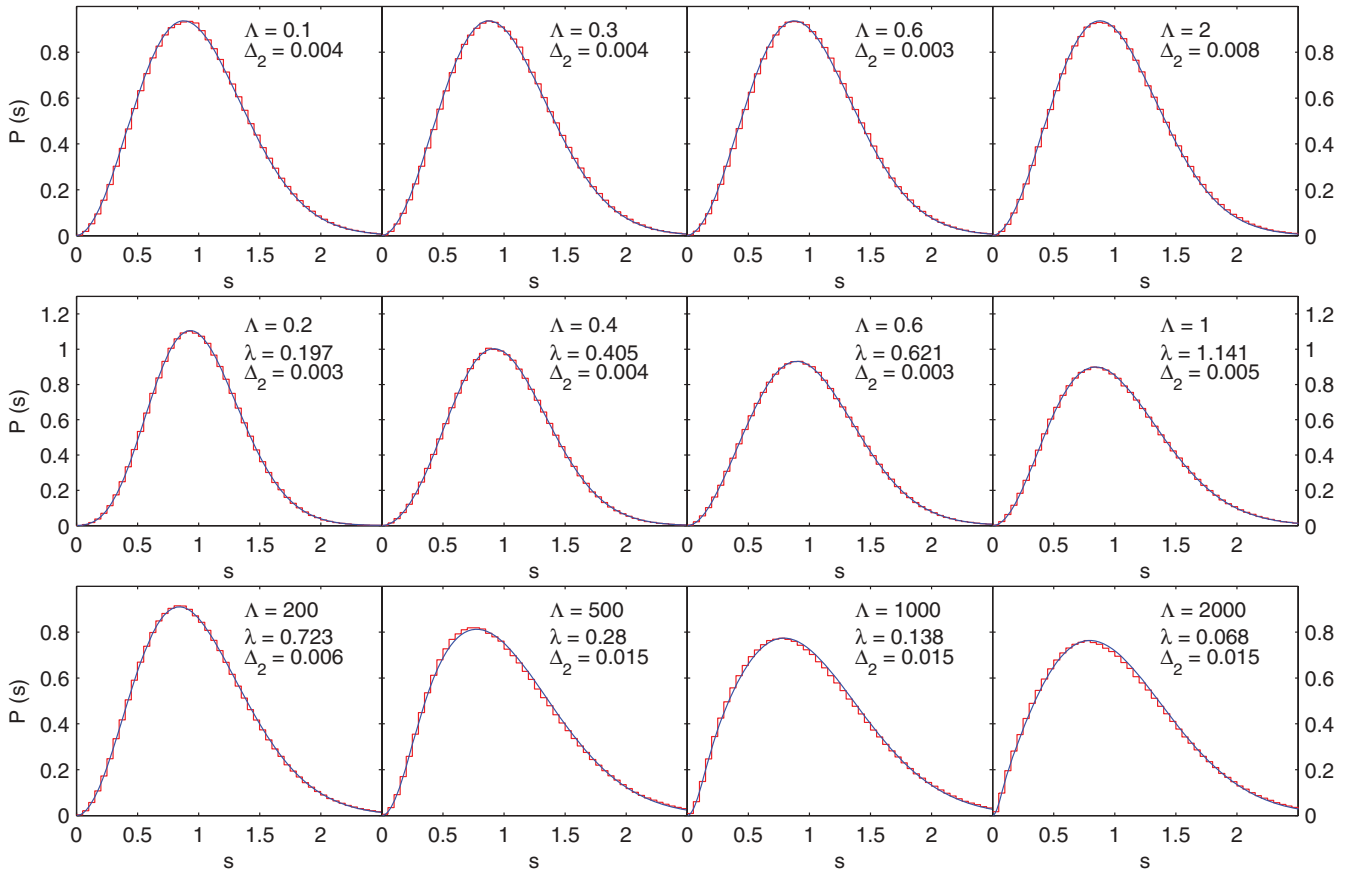
FIG. 10. (Color online) Spacing distributions for the transition GSE $\to$ GOE without self-dual symmetry for various values of the coupling parameter Λ in Eq. (3.17). Top: Spacings s_1 between previously degenerate eigenvalues (for small Λ). Middle: Spacings s_2 between previously nondegenerate eigenvalues (also for small Λ). Bottom: All spacings (for large Λ). The histograms show the numerical data, while the full curves are the 2×2 GUE surmise P_2 (top), the surmise $P_{4 \to 1}^2(s_2; \lambda)$ given in Eq. (3.19) (middle), and the surmise $P_{1 \to 2}(s; \lambda)$ given in Eq. (2.33), the latter two with fitted coupling parameter λ. The quantity Δ_2 defined in Appendix F is a measure of the fit quality, which is small for a good fit. The numerical data were obtained by diagonalizing 50 000 random matrices of dimension 400 for each plot.

case of Poisson) was broken or restored. In contrast, we now have two transitions. As Λ increases from zero, an antiunitary symmetry T with $T^2 = -\mathbb{1}$ gets broken. As Λ decreases from infinity, either an antiunitary symmetry with $T^2 = \mathbb{1}$ gets broken (in the case of GOE) or integrability gets broken (in the case of Poisson). For intermediate values of Λ the system follows GUE statistics because all antiunitary symmetries and/or integrability are broken. This is illustrated in Fig. 11.
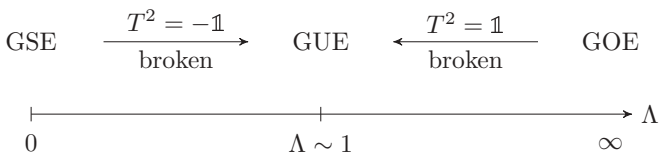

FIG. 11. Schematic picture of the transition from GSE to non-self-dual GOE, which proceeds via an intermediate transition to the GUE. An analogous picture applies to the transition from GSE to non-self-dual Poisson.

IV. SUMMARY

We have derived generalized Wigner surmises for the nearest-neighbor spacing distributions of various mixed RMT ensembles from 2×2 and 4×4 matrices. If the GSE was involved in the transition, we have distinguished two cases: (i) perturbations of the GSE by a self-dual ensemble and (ii) perturbations of the GSE by a non-self-dual ensemble, for which we separately considered two different kinds of spacings.

We have shown that all of these distributions yield a good description of the spectra of large mixed matrices when restricted to a range of constant spectral density. The coupling parameters in the generalized Wigner surmise and in the large mixed matrices are related via the local eigenvalue density of the latter. This relation is well approximated by Eq. (3.7).

We expect that the results for $P(s)$ derived in this paper will be useful in numerical and/or experimental studies of systems with mixed symmetries, such as those mentioned in Sec. I. $P(s)$ is a convenient quantity that is easily analyzed numerically or experimentally and typically does not suffer from serious unfolding issues. In particular, the properties of the level spacings should help us to clarify whether the mixing of the symmetry classes in a given physical system is of the

additive type (1.4) we have investigated here. If so, fits to the generalized Wigner surmises provide estimates of the coupling parameter in terms of the local eigenvalue density. In turn, the coupling parameter could quantify other properties of the mixed systems.

APPENDIX A: ANALYSIS OF THE LARGE-s BEHAVIOR

We consider the large-s behavior of the spacing distributions for the three transitions from Poisson to RMT. For simplicity, we first consider the non-normalized spacing S and convert to the normalized spacing s at the end. We start with the initial ansatz for the distributions,

$$I(S) = \int dp\, da\, db \prod_{\nu=0}^{\beta-1} dc_\nu\, P_0(p) P_a(a) P_b(b) P_{c_\nu}(c_\nu)$$

$$\times \delta\left(S - \sqrt{[a-(b+p/\lambda)]^2 + 4\sum_{\mu=0}^{\beta-1} c_\mu c_\mu}\right),$$
(A1)

which is the generalization of Eq. (2.23) to $\beta = 1$, 2, and 4. As in Appendix C 1, we introduce new variables $u = a + b$ and $t = a - b$, transform the c_ν to spherical coordinates, and eliminate the δ function by integrating out the radius. This yields

$$I(S) \sim \int_0^\infty dp \int_{-S}^{S} dt\, (S^2 - t^2)^{\frac{\beta}{2}-1} S e^{-\frac{p^2}{4\lambda^2} - p - \frac{pt}{2\lambda} - \frac{1}{4}S^2}$$

$$\sim S^\beta e^{-\frac{1}{4}S^2} \int_0^\infty dp\, e^{-p^2 - 2\lambda p} \int_{-1}^{1} dx\, (1-x^2)^{\frac{\beta}{2}-1} e^{-pxS}$$

$$\sim S^\beta e^{-\frac{1}{4}S^2} \int_0^\infty dp\, e^{-p^2 - 2\lambda p} X_\beta(pS),$$
(A2)

where we substituted $t = xS$, rescaled $p \to 2\lambda p$, and expressed the x integral (up to normalization) as

$$X_\beta(pS) = (pS)^{-\frac{\beta-1}{2}} I_{\frac{\beta-1}{2}}(pS),$$
(A3)

where I is a modified Bessel function [[35], Eq. (9.6.18)]. We now compute the integral in Eq. (A2) in saddle-point approximation, assuming S to be large. The asymptotic expansion of X_β for $\beta = 1,2,4$ reads

$$X_\beta(pS) = \frac{1}{\sqrt{2\pi}} (pS)^{-\frac{\beta}{2}} e^{pS}.$$
(A4)

For $p = O(S^{-1})$ we cannot use this expansion, but the contribution of this region to the integral can be shown to be negligible compared to the leading order we consider here. The exponential in the integrand is now

$$e^{-p^2 - 2\lambda p + pS},$$
(A5)

with a maximum at $p_{\max} = S/2 - \lambda$. Standard manipulations then yield the saddle-point result

$$I(S) \sim e^{-\lambda S}[1 + O(S^{-1})].$$
(A6)

The normalized distributions are obtained from $I(S)$ by rescaling the spacing and restoring the normalization factors that were omitted in the calculation above, resulting in

$$P_{0\to\beta}(s;\lambda) = e^{-2\lambda Ds}[2\lambda D e^{\lambda^2} + O(s^{-1})],$$
(A7)

where we replaced S by $2Ds$ with D given in Eqs. (2.5), (2.13), and (2.27) for $\beta = 1,2,4$, respectively. The meaning of this result is that for arbitrarily large (but finite) λ, i.e., arbitrarily close to the pure Gaussian ensemble, the large-s behavior is Poisson-like. This is in contrast to the small-s behavior, which is dominated by the Gaussian ensemble for arbitrarily small (but nonzero) λ. The findings for the large-s behavior were also confirmed numerically.

APPENDIX B: ANALYSIS OF THE GIBBS PHENOMENON

The spacing distribution of ensembles interpolating between Poisson and RMT reveal a Gibbs-like phenomenon close to the Poisson limit, i.e., for small λ: $P(s;\lambda)$ does not converge uniformly to the Poisson curve e^{-s} at $s = 0$. Rather, there is an overshoot whose amount does not vanish in the $\lambda \to 0$ limit and whose position s approaches 0 in this limit. In this Appendix we work out the value and position of this maximum. We start with a brief review of the Gibbs phenomenon in the Fourier transform, as known from textbooks such as [43] (which, however, mostly discuss the Gibbs phenomenon only in the Fourier series).

1. Gibbs phenomenon in the Fourier transform

The Gibbs phenomenon is related to the convergence of the inverse Fourier transform with a cutoff in the integral (or to the convergence of the Fourier series with a cutoff in the sum) toward the original function f. Let us denote its Fourier transform by F,

$$F(\omega) = \frac{1}{2\pi} \int_{-\infty}^{\infty} ds\, e^{-i\omega s} f(s),$$
(B1)

and the result of the cutoff inverse transform by f with two arguments,

$$f(s;\lambda) = \int_{-1/\lambda}^{1/\lambda} d\omega\, e^{i\omega s} F(\omega).$$
(B2)

These formulas can be combined into a convolution

$$f(s;\lambda) = \int_{-\infty}^{\infty} ds'\, f(s') \delta_\lambda(s - s')$$
(B3)

of the original function with the Dirichlet kernel

$$\delta_\lambda(s - s') = \frac{1}{2\pi} \int_{-1/\lambda}^{1/\lambda} d\omega\, e^{i\omega(s-s')} = \frac{\sin[(s-s')/\lambda]}{\pi(s - s')}.$$
(B4)

The question is how $f(s;\lambda)$ is related to the original function $f(s)$ in the $\lambda \to 0$ limit.[7] If $f(s)$ is smooth and absolutely

----

[7]The $\lambda \to 0$ limit of $f(s;\lambda)$ is also denoted as the principal value.

integrable, $f(s;\lambda)$ approaches it everywhere. Accordingly, the Dirichlet kernel approaches the delta distribution in the sense of acting on smooth test functions.

At discontinuities of the original function $f(s)$, however, $f(s;\lambda)$ approaches the average of the left and right limits of $f(s)$. Intuitively, this comes from the nonzero width of the Dirichlet kernel,[8] which in the convolution (B3) probes both sides of the discontinuity. Furthermore, the functions $f(s;\lambda)$ for fixed λ possess maxima and minima whose positions move, in the limit $\lambda \to 0$, toward the discontinuity and whose values over- and undershoot the function. This is the Gibbs phenomenon.

For definiteness let us consider a set of exponentially decaying functions with a jump discontinuity of unit size[9] at $s = 0$,

$$f(s) = \begin{cases} 0 & \text{for} \quad s < 0, \\ e^{-ds} & \text{for} \quad s > 0, \end{cases} \tag{B5}$$

that include the Poisson curve ($d = 1$) and the Heaviside function ($d = 0$). The Fourier transforms are

$$F(\omega) = \frac{1}{2\pi} \frac{1}{d + i\omega}, \tag{B6}$$

and the cutoff inverse transforms read

$$f(s;\lambda) = \frac{i}{2\pi} e^{-ds} \left[\text{Ei}\left(ds - i\frac{s}{\lambda}\right) - \text{Ei}\left(ds + i\frac{s}{\lambda}\right) \right]. \tag{B7}$$

For the Poisson curve these functions are plotted for three small values of λ in Fig. 12 (top), where several maxima above and several minima below e^{-s} are clearly visible.

To analyze the limit $\lambda \to 0$ we can zoom in on the region of small s, of size proportional to λ. This amounts to considering functions of a rescaled argument

$$\tilde{s} = \frac{s}{\lambda} \tag{B8}$$

in a constant-$\tilde{s}$ range. We define

$$\hat{f}(\tilde{s};\lambda) = f(\tilde{s}\lambda;\lambda)$$
$$= \frac{i}{2\pi} e^{-d\tilde{s}\lambda} [\text{Ei}(d\tilde{s}\lambda - i\tilde{s}) - \text{Ei}(d\tilde{s}\lambda + i\tilde{s})]. \tag{B9}$$

If we keep $\tilde{s}$ fixed, these functions have a well-defined limit as $\lambda \to 0$,

$$g(\tilde{s}) = \lim_{\lambda \to 0} \hat{f}(\tilde{s};\lambda)$$
$$= \frac{i}{2\pi} [\text{Ei}(-i\tilde{s}) - \text{Ei}(i\tilde{s})] = \frac{1}{2} + \frac{\text{Si}(\tilde{s})}{\pi}, \tag{B10}$$

with the sine integral $\text{Si}(\tilde{s}) = \int_0^{\tilde{s}} dx \, \sin x / x$. As Fig. 12 (bottom) shows, this limiting function captures infinitely many maxima at $\tilde{s} = \pi, 3\pi, \ldots$ and infinitely many minima at $\tilde{s} = 2\pi, 4\pi, \ldots$. The overshoot at the first maximum is the well-known number

$$\frac{1}{2} + \frac{\text{Si}(\pi)}{\pi} - 1 = 0.0894899. \tag{B11}$$

---

[8]This nonzero width is relevant in many areas of physics such as band-limited signals, ringing, and diffraction of waves at slits.

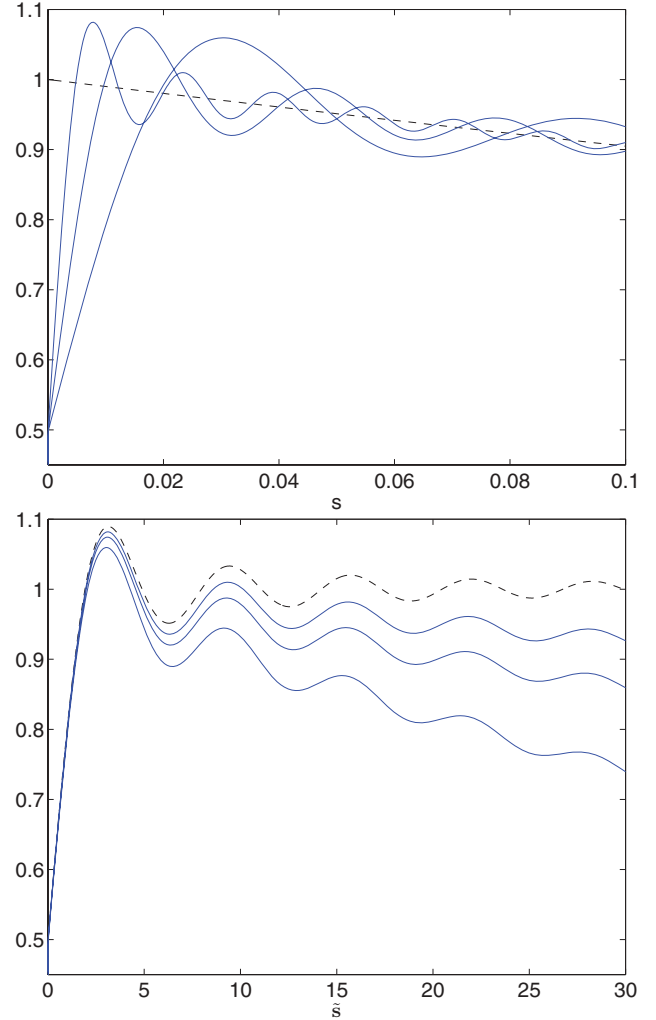[9]As all formulas are linear in $f(s)$, the case of arbitrary jumps is completely analogous.

FIG. 12. (Color online) The Gibbs phenomenon in the Fourier transform of the Poisson curve, with $\lambda = 0.01, 0.005, 0.0025$, respectively. Top: The functions $f(s;\lambda)$ approaching the original function e^{-s} (dashed), first maximum moving to the left as λ decreases. Bottom: The rescaled functions $\hat{f}(\tilde{s};\lambda)$ approaching the limiting function $g(\tilde{s})$ (dashed) with decreasing λ (see text).

Concerning the convergence of the Fourier transform, we conclude that in the limit $\lambda \to 0$ the functions $f(s;\lambda)$ have a maximum at $s = \pi\lambda$, with an overshoot approaching 8.9%.

Note that the limiting function g is the same for all these functions independently of the decay constants d; i.e., it is solely determined by the discontinuity. In other words, the smooth part of the function $f(s)$ drops out when going from $\hat{f}(\tilde{s};\lambda)$ to $g(\tilde{s})$ in the $\lambda \to 0$ limit [see Eq. (B9) versus Eq. (B10)]. This can be shown to be universal. Rescaling the integration variable in Eq. (B3) and using $\lambda\delta_\lambda(\lambda x) = \delta_1(x)$ one has

$$f(s;\lambda) = \int_0^\infty ds'' \, f(\lambda s'') \delta_1\left(\frac{s}{\lambda} - s''\right), \tag{B12}$$

$$\hat{f}(\tilde{s};\lambda) = \int_0^\infty ds'' \, f(\lambda s'') \delta_1(\tilde{s} - s''), \tag{B13}$$

where we still assume $f(s < 0) = 0$ for simplicity. The limiting function is

$$g(\tilde{s}) = f(0^+) \int_{-\infty}^{\tilde{s}} dt \, \delta_1(t) = f(0^+) \left[\frac{1}{2} + \frac{\text{Si}(\tilde{s})}{\pi} \right], \quad \text{(B14)}$$

which agrees with (B10) for all functions with $f(0^+) = 1$.

The last equation in particular relates the Dirichlet kernel δ_λ and the limiting function g. Therefore, $f(s; \lambda)$ can also be reconstructed by a convolution with (the derivative of) g,

$$f(s; \lambda) = \int_0^\infty ds' \, f(s') \frac{1}{\lambda} g' \left(\frac{s - s'}{\lambda} \right), \quad \text{(B15)}$$

where $g'(x) = dg/dx$.

2. Gibbs phenomenon in the Poisson to RMT transitions

For the Gibbs-like phenomenon in the mixed spacing distributions we start with the Poisson to GSE case. For this transition we found the spacing distribution Eq. (2.26). In analogy to the previous section we rescale the argument and define

$$\hat{P}_{0 \to 4}(\tilde{s}; \lambda)$$
$$= P_{0 \to 4}(\tilde{s}\lambda; \lambda) = C\lambda^4 \tilde{s}^4 e^{-D^2 \lambda^2 \tilde{s}^2}$$
$$\times \int_{-1}^{1} dx \, (1 - x^2) \, e^{(xD\lambda\tilde{s})^2 + 2\lambda^2 xD\tilde{s}} \, \text{erfc}(xD\lambda\tilde{s} + \lambda). \quad \text{(B16)}$$

In the limit $\lambda \to 0$ we make use of the behavior of $C(\lambda)$ and $D(\lambda)$,

$$D(\lambda) \sim \frac{1}{2\lambda} \quad \text{and} \quad C(\lambda) \sim \frac{1}{(2\lambda)^4}, \quad \text{(B17)}$$

to arrive at the limiting function

$$g_{0 \to 4}(\tilde{s}) = \lim_{\lambda \to 0} \hat{P}_{0 \to 4}(\tilde{s}; \lambda)$$
$$= \frac{\tilde{s}^4}{16} e^{-\frac{\tilde{s}^2}{4}} \int_{-1}^{1} dx \, (1 - x^2) \, e^{(x\tilde{s}/2)^2} \, \text{erfc} \, \frac{x\tilde{s}}{2}$$
$$= \frac{\tilde{s}}{8} [(2 + \tilde{s}^2)\sqrt{\pi} e^{-\frac{\tilde{s}^2}{4}} \, \text{erfi}(\tilde{s}/2) - 2\tilde{s}]. \quad \text{(B18)}$$

In Fig. 13 we plot this function, together with $\hat{P}_{0 \to 4}(\tilde{s}; \lambda)$, approaching it for small λ.

Again, this limiting function captures a maximum, which can numerically be determined to be at $\tilde{s} = 3.76023$ with a value of 1.43453. As before, the phenomenon is solely determined by the discontinuity of the Poisson curve at $s = 0$ as the original Poisson distribution e^{-p} can be shown to drop out from Eqs. (B16) to (B18).

So in the transition from Poisson to GSE, $P_{0 \to 4}(s; \lambda)$ in the limit of small λ has a maximum at $s = 3.76\lambda$, overshooting the Poissonian e^{-s} by 43.5%. Likewise, in the other transitions $P_{0 \to 1}(s; \lambda)$ and $P_{0 \to 2}(s; \lambda)$ we have equivalently defined limiting functions

$$g_{0 \to 1}(\tilde{s}) = \frac{\sqrt{\pi}}{2} \tilde{s} \, e^{-\tilde{s}^2/8} \, I_0(\tilde{s}^2/8), \quad \text{(B19)}$$

$$g_{0 \to 2}(\tilde{s}) = \frac{\sqrt{\pi}}{2} \tilde{s} \, e^{-\tilde{s}^2/4} \, \text{erfi}(\tilde{s}/2). \quad \text{(B20)}$$
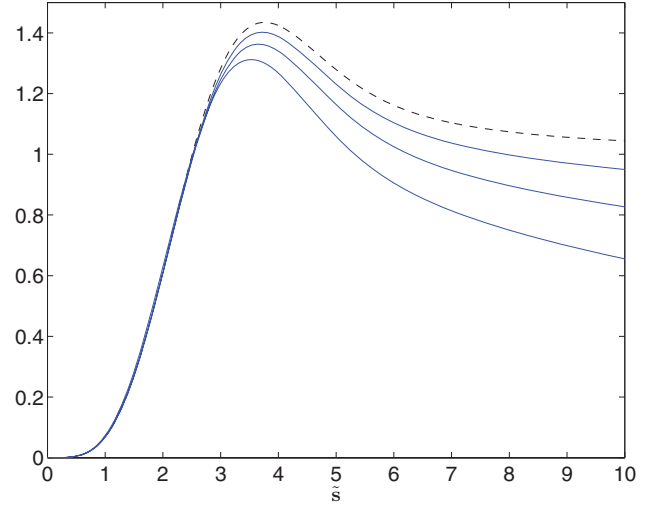

FIG. 13. (Color online) The rescaled spacing distributions $\hat{P}_{0 \to 4}(\tilde{s}; \lambda)$ in the Poisson to GSE transition, Eq. (B16), for $\lambda = 0.05, 0.025, 0.01$ (maxima increasing) approaching the limiting function $g_{0 \to 4}(\tilde{s})$, Eq. (B18) (dashed curve).

These have maxima at $\tilde{s} = 2.51$ and $\tilde{s} = 3.00$, overshooting the Poisson curve by 17.5% and 28.5%, respectively, as quoted in the body of the paper. We observe that these numbers grow with the Dyson index β' of the perturbing ensemble.

From the small-$\tilde{s}$ behavior $g_{0 \to 4}(\tilde{s}) = \tilde{s}^4/12 + O(\tilde{s}^6)$ we conclude that $P_{0 \to 4}(s; \lambda) = s^4/(12\lambda^4) + O(s^6)$ for small λ, which reproduces our observation in Eqs. (2.30) and (2.31). Analogous agreement is obtained with Eqs. (2.9), (2.10), (2.19), and (2.20) for the other two cases. This concludes our empirical results on the Gibbs-like phenomenon.

For the analogies at a more fundamental level, the spacing distribution $P_{0 \to 4}(s; \lambda)$ is related to the integral (2.23)

$$\frac{1}{\lambda} I(S/\lambda) = \int_0^\infty dp \, e^{-p} \, \delta_\lambda(S, p) \quad \text{(B21)}$$

of the unperturbed Poisson distribution with the kernel

$$\delta_\lambda(S, p) = \int da \ldots dc_3 \, P_a(a) \ldots P_{c_3}(c_3)$$
$$\times \delta(S - \lambda \sqrt{(a - b - p/\lambda)^2 + 4(c_\mu c_\mu)}). \quad \text{(B22)}$$

The nonzero width of this kernel causes the Gibbs phenomenon in the spacing distribution near the discontinuity of the Poisson distribution e^{-p} at $p = 0$. Note that in the limit $\lambda \to 0$ the second line of Eq. (B22) approaches $\delta(S - p)$, thus decoupling from the integrals over $a, \ldots, c_3$. The latter are normalized by construction so that the kernel $\delta_\lambda(S, p)$ approaches $\delta(S - p)$.

There are (at least) two features that are different from the Fourier case. First, the kernel is not a function of $S - p$, and thus Eq. (B21) is not a convolution, in contrast to the Fourier case, Eq. (B15). Second, at the discontinuity $P_{0 \to 4}(0; \lambda) = 0$ is not the average (equal to 1/2) of the left and right limits of the original Poisson curve e^{-p} (put to zero for negative p).

APPENDIX C: EXPLICIT CALCULATION OF SPACING DISTRIBUTIONS

1. Poisson to GSE

We start from Eq. (2.25), transform $c_0, \ldots, c_3$ to spherical coordinates with $c^2 = c_\mu c_\mu$, and introduce $u = a + b$ and $t = a - b$. This yields

$$
I(S) \propto \int_0^\infty dp \, dc \, c^3 \int_{-\infty}^\infty du \, dt \, e^{-p - \frac{1}{4}(u^2 + t^2) + \frac{p(u-t)}{2\lambda} - \frac{p^2}{2\lambda^2} - c^2}
$$
$$
\times \, \delta(S - \sqrt{t^2 + 4c^2})
$$
$$
\propto \int_0^\infty dp \, dc \, c^3 \int_{-\infty}^\infty dt \, e^{-p - \frac{pt}{2\lambda} - \frac{p^2}{4\lambda^2} - \frac{1}{4}(t^2 + 4c^2)}
$$
$$
\times \, \delta(S - \sqrt{t^2 + 4c^2}), \tag{C1}
$$

where in the last step we have integrated over u. We now use the δ function to integrate over c, resulting in

$$
I(S) \propto S \, e^{-\frac{S^2}{4}} \int_0^\infty dp \, e^{-\frac{p^2}{4\lambda^2} - p} \int_{-S}^S dt \, (S^2 - t^2) e^{-\frac{pt}{2\lambda}}
$$
$$
\propto S^4 \, e^{-\frac{S^2}{4}} \int_0^\infty dp \, e^{-\frac{p^2}{4\lambda^2} - p} \, \frac{z \cosh z - \sinh z}{z^3}
$$
$$
\equiv J(S), \tag{C2}
$$

where $z = pS/2\lambda$.

The normalized level spacing distribution $P_{0 \to 4}(s)$, Eq. (2.26), is obtained from $J(S)$ by rescaling and normalization, i.e., $P_{0 \to 4}(s) = C \cdot J(2Ds)/(2D)^4$. Defining the moments of the distribution,

$$
\mathcal{I}_n = \int_0^\infty dS \, S^n J(S), \tag{C3}
$$

we obtain from Eq. (1.2)

$$
D = \frac{\mathcal{I}_1}{2\mathcal{I}_0} \quad \text{and} \quad C = \frac{(2D)^5}{\mathcal{I}_0}. \tag{C4}
$$

Explicit evaluation of $\mathcal{I}_0$ and $\mathcal{I}_1$ gives

$$
\mathcal{I}_0 = 4\sqrt{\pi}, \tag{C5}
$$

$$
\mathcal{I}_1 = 4\lambda \int_0^\infty dx \, e^{-2\lambda x}
$$
$$
\times \, \frac{(4x^3 + 2x)e^{-x^2} + \sqrt{\pi}(4x^4 + 4x^2 - 1)\,\text{erf}(x)}{x^3}, \tag{C6}
$$

from which we obtain Eqs. (2.27) and (2.28).

2. GOE to GSE

We consider the matrix H in Eq. (2.40). With a small change in notation for H_1, we have

$$
H = H_1 \otimes \mathbb{1}_2 + \lambda H_4 = \begin{pmatrix} A & 0 & C & 0 \\ 0 & A & 0 & C \\ C & 0 & B & 0 \\ 0 & C & 0 & B \end{pmatrix}
$$

$$
+ \lambda \begin{pmatrix} a & 0 & c_0 + ic_3 & c_1 + ic_2 \\ 0 & a & -c_1 + ic_2 & c_0 - ic_3 \\ c_0 - ic_3 & -c_1 - ic_2 & b & 0 \\ c_1 - ic_2 & c_0 + ic_3 & 0 & b \end{pmatrix}, \tag{C7}
$$

where the variances of the random variables are given by Eq. (2.2). If two variables are Gaussian distributed with variances σ_1^2 and σ_2^2, their sum is again Gaussian distributed with variance $\sigma_1^2 + \sigma_2^2$. Since H depends on A, B, and C and a, b, and c_0 only through the combinations $A + \lambda a$, $B + \lambda b$, and $C + \lambda c_0$, we can immediately integrate out A, B, and C, with the corresponding change in the variances of a, b, and c_0. To simplify the notation, we absorb λ in H_4 and divide all matrix elements of H by $\sqrt{1 + \lambda^2}$. This yields a problem equivalent to Eq. (C7),

$$
H \to \begin{pmatrix} a & 0 & c_0 + ic_3 & c_1 + ic_2 \\ 0 & a & -c_1 + ic_2 & c_0 - ic_3 \\ c_0 - ic_3 & -c_1 - ic_2 & b & 0 \\ c_1 - ic_2 & c_0 + ic_3 & 0 & b \end{pmatrix}, \tag{C8}
$$

with

$$
\sigma_{a,b}^2 = 2\sigma_{c_0}^2 = 1, \quad 2\sigma_{c_i}^2 = \frac{\lambda^2}{1 + \lambda^2} \equiv \sigma^2, \tag{C9}
$$

where $i = 1, 2, 3$. The matrix in Eq. (C8) has two nondegenerate eigenvalues whose spacing is given by

$$
S = \left[(a - b)^2 + 4 \sum_{\nu=0}^3 c_\nu c_\nu \right]^{1/2}, \tag{C10}
$$

where we have again written S instead of s since we still need to enforce the normalizations (1.2). The spacing distribution is proportional to the integral

$$
I(S) = \int_{-\infty}^\infty da \, db \, dc_0 dc_1 dc_2 dc_3 \, e^{-\frac{1}{2}(a^2 + b^2 + 2c_0^2) - \frac{c_i c_i}{\sigma^2}}
$$
$$
\times \, \delta\big(S - \sqrt{(a-b)^2 + 4c_0^2 + 4c_j c_j}\big), \tag{C11}
$$

where repeated indices indicate a sum over i and j from 1 to 3. We now transform c_1, c_2, c_3 to spherical coordinates with $c^2 = c_i c_i$ and introduce $u = a + b$ and $t = a - b$. This yields

$$
I(S) \propto \int_{-\infty}^\infty du \, dt \, dc_0 dc \, c^2 \, e^{-\frac{1}{4}(u^2 + t^2 + 4c_0^2) - \frac{c^2}{\sigma^2}}
$$
$$
\times \, \delta\big(S - \sqrt{t^2 + 4c_0^2 + 4c^2}\big). \tag{C12}
$$

The integral over u can be performed trivially and only results in a prefactor. Using the δ function to integrate over c, we obtain

$$
I(S) \propto \int_0^\infty dt \, dc_0 \, e^{-\frac{1}{4}(t^2 + 4c_0^2) - \frac{1}{4\sigma^2}(S^2 - t^2 - 4c_0^2)}
$$
$$
\times \, S\sqrt{S^2 - t^2 - 4c_0^2} \, \theta\big(S^2 - t^2 - 4c_0^2\big), \tag{C13}
$$

where we have used the symmetries of the integrand to raise the lower limit of the integrations to zero. We now perform the transformation

$$
t = Sx \quad \text{and} \quad c_0 = \tfrac{1}{2}Sy\sqrt{1 - x^2} \tag{C14}
$$

with Jacobian $\frac{1}{2}S^2\sqrt{1-x^2}$. Since t and c_0 are non-negative, so are x and y. The θ function in Eq. (C13) then implies $0 \leqslant x, y \leqslant 1$. Reinserting the definition of σ^2 from Eq. (C9), we obtain

$$I(S) \propto S^4 \int_0^1 dx\, dy\,(1-x^2)\sqrt{1-y^2}e^{-\frac{S^2}{4\lambda^2}[\lambda^2+(1-x^2)(1-y^2)]}.$$

(C15)

We now substitute $y = \cos\phi$, note that $\cos^2\phi = \frac{1}{2}(1-\cos 2\phi)$, and use the integral representation [[35], Eq. (9.6.19)] of the modified Bessel functions I_0 and I_1 to obtain after some algebra

$$I(S) \propto S^4 e^{-\frac{1+2\lambda^2}{8\lambda^2}S^2} \int_0^1 dx\,(1-x^2)\,e^{\frac{S^2 x^2}{8\lambda^2}}[I_0(z)-I_1(z)]$$
$$\equiv J(S),$$

(C16)

with $z = (1-x^2)S^2/(8\lambda^2)$. This corresponds to Eq. (2.41) with $S = \sqrt{8}\lambda Ds$. The properly normalized spacing distribution is therefore given by $P_{1\to 4}(s) = CJ(\sqrt{8}\lambda Ds)/(\sqrt{8}\lambda D)^4$. Defining

$$\mathcal{I}_n = \int_0^\infty dS\, S^n J(S)$$

(C17)

we obtain from Eq. (1.2)

$$D = \frac{\mathcal{I}_1}{\sqrt{8}\lambda \mathcal{I}_0} \quad \text{and} \quad C = \frac{(\sqrt{8}\lambda D)^5}{\mathcal{I}_0}.$$

(C18)

Explicit evaluation of $\mathcal{I}_0$ and $\mathcal{I}_1$ gives

$$\mathcal{I}_0 = 8\sqrt{\pi}\left(\frac{\lambda^2}{1+\lambda^2}\right)^{3/2},$$

(C19)

$$\mathcal{I}_1 = 16\lambda^3\left[\frac{\lambda(1-\lambda^2)}{(1+\lambda^2)^2}+\operatorname{arccot}\lambda\right],$$

(C20)

from which we obtain Eqs. (2.42) and (2.43).

APPENDIX D: PERTURBATION OF A LARGE GSE MATRIX BY A NON-SELF-DUAL MATRIX

We consider a mixed $2N \times 2N$ matrix that interpolates between the GSE and one of the other Gaussian ensembles,

$$H = H_4 + \frac{\Lambda}{\rho_4(0)\bar{s}_4}H_{\beta'},$$

(D1)

where H_4 is taken from the GSE and $H_{\beta'}$ from the GOE or GUE. We study this matrix for large N in first-order degenerate perturbation theory to show similarities between the two different perturbations and to make a connection to the case of GSE to non-self-dual GUE for $N = 2$, which was treated in Sec. II H.

Degenerate perturbation theory predicts that each of the N previously degenerate eigenvalue pairs splits up and that the shifts of the two members of the pair are the eigenvalues of the matrix

$$\frac{\Lambda}{\rho_4(0)\bar{s}_4}M_{ij} \quad \text{with} \quad M_{ij} = \langle\psi_i|H_{\beta'}|\psi_j\rangle; \quad i,j = 1,2. \quad (D2)$$

The $|\psi_{1,2}\rangle$ are the orthonormal eigenvectors of the unperturbed matrix H_4 that span the degenerate subspace of the eigenvalue pair under consideration.

We show in the following that M is a 2×2 GUE matrix for $\beta' = 2$ as well as for $\beta' = 1$, in the latter case with a normalization different from Eq. (2.2).

1. GUE

This case is very simple, because the GUE is invariant under unitary transformations, which contain the symplectic transformations. This means that the transformation diagonalizing the GSE matrix H_4 can be absorbed in H_2 without loss of generality, and therefore one can choose $|\psi_i\rangle_k = \delta_{ik}$ with $i = 1,2$ and $k = 1,\dots,2N$. Thus, we obtain

$$M_{ij} = \sum_{k,l=1}^{2N} \delta_{ik}\,(H_2)_{kl}\,\delta_{lj} = (H_2)_{ij},$$

(D3)

which is obviously a 2×2 matrix from the GUE with the usual normalization, Eq. (2.2). As this holds also for $N = 2$, it is a perturbative explanation for the fact that in the limit $\lambda \to 0$ the spacings between previously degenerate eigenvalues are distributed exactly like the ones of 2×2 GUE matrices.

2. GOE

We will show that in this case M is again a matrix from the GUE with the only difference that the variances of its elements are only half as large as in the previous section. This case is a bit more involved because one cannot generally diagonalize a self-dual matrix by an orthogonal transformation (which would preserve the probability distribution of H_1), and thus it is impossible to choose the eigenvectors of H_4 as in the previous section. Explicitly, the matrix elements read

$$M_{ij} = \langle\psi_i|H_1|\psi_j\rangle = \langle\psi_i^{\rm re}|H_1|\psi_j^{\rm re}\rangle + \langle\psi_i^{\rm im}|H_1|\psi_j^{\rm im}\rangle$$
$$+ i\left(\langle\psi_i^{\rm re}|H_1|\psi_j^{\rm im}\rangle - \langle\psi_i^{\rm im}|H_1|\psi_j^{\rm re}\rangle\right),$$

(D4)

where we split the eigenvectors $|\psi_i\rangle$ into real and imaginary parts: $|\psi_i\rangle = |\psi_i^{\rm re}\rangle + i|\psi_i^{\rm im}\rangle$, and H_1 is real.

We will now show that the four vectors $|\psi_1^{\rm re}\rangle$, $|\psi_1^{\rm im}\rangle$, $|\psi_2^{\rm re}\rangle$, and $|\psi_2^{\rm im}\rangle$ are orthogonal in the limit of infinite matrix size. For some combinations of them one can show this also for finite N using the quaternionic structure of the eigenvectors,

$$\begin{pmatrix}\langle\psi_1|\\\langle\psi_2|\end{pmatrix} = (q_1\ q_2\ \cdots\ q_N),$$

(D5)

with quaternions in matrix representation

$$q_k = \begin{pmatrix} q_k^{(0)}+iq_k^{(3)} & q_k^{(1)}+iq_k^{(2)} \\ -q_k^{(1)}+iq_k^{(2)} & q_k^{(0)}-iq_k^{(3)} \end{pmatrix}.$$

(D6)

One can read off immediately that

$$\langle\psi_1^{\rm re}|\psi_2^{\rm re}\rangle = \langle\psi_1^{\rm im}|\psi_2^{\rm im}\rangle = 0,$$

(D7)

$$\langle\psi_1^{\rm re}|\psi_1^{\rm im}\rangle = -\langle\psi_2^{\rm re}|\psi_2^{\rm im}\rangle,$$

(D8)

$$\langle\psi_1^{\rm re}|\psi_2^{\rm im}\rangle = \langle\psi_1^{\rm im}|\psi_2^{\rm re}\rangle;$$

(D9)

i.e., there are only two independent scalar products.

Let us assume that for large N the $q_k^{(\rho)}$ can be treated as independent random variables with mean value zero. Then the

mean values of those scalar products are zero as well, e.g.,

$$\langle\langle\psi_1^{\mathrm{re}}|\psi_1^{\mathrm{im}}\rangle\rangle = \sum_{k=1}^{N}\langle q_k^{(0)}q_k^{(3)} + q_k^{(1)}q_k^{(2)}\rangle = 0, \quad \text{(D10)}$$

where the outer angular brackets indicate an average over the random matrix ensemble. From the normalization of the eigenvectors $|\psi_i\rangle$ the variances of the $q_k^{(\rho)}$ are proportional to $1/N$. This yields for the variances of the scalar products

$$\langle\langle\psi_1^{\mathrm{re}}|\psi_1^{\mathrm{im}}\rangle^2\rangle = \sum_{k=1}^{N}\left(\langle[q_k^{(0)}]^2\rangle\langle[q_k^{(3)}]^2\rangle + \langle[q_k^{(1)}]^2\rangle\langle[q_k^{(2)}]^2\rangle\right)$$

$$\propto \sum_{k=1}^{N}\frac{1}{N^2} = \frac{1}{N} \quad \text{(D11)}$$

and likewise for $\langle\psi_1^{\mathrm{re}}|\psi_2^{\mathrm{im}}\rangle$. Since in the $N \to \infty$ limit both the mean values and the variances of the scalar products vanish, the four vectors become orthogonal in this limit for every single realization of the random matrix. We have checked this numerically, which implies that the assumption of the independence of the $q_k^{(\rho)}$ was valid.

As for the normalization of the four vectors, the squared norms of the real and imaginary parts agree on average and sum up to 1 due to the normalization of the eigenvectors $|\psi_i\rangle$. Invoking the central limit theorem, we observe that in the limit $N \to \infty$ the norms of the real and imaginary parts equal $1/\sqrt{2}$ even for a single realization of the random matrix. Hence, multiplying the four real vectors $|\psi_1^{\mathrm{re}}\rangle$, $|\psi_1^{\mathrm{im}}\rangle$, $|\psi_2^{\mathrm{re}}\rangle$, and $|\psi_2^{\mathrm{im}}\rangle$ by $\sqrt{2}$, one obtains, in the limit $N \to \infty$, an orthonormal real basis in the subspace under consideration.

Finally, we use the fact that the matrix elements of a GOE matrix H_1 are independent random numbers *in every orthonormal (real) basis*, with variances 1 and 1/2 on and off the diagonal, respectively. Thus we conclude that the M_{ij} are also independent random numbers with variances

$$\langle\left[M_{11}^{\mathrm{re}}\right]^2\rangle = \langle\left[M_{22}^{\mathrm{re}}\right]^2\rangle = \tfrac{1}{2}, \quad \text{(D12)}$$

$$\langle\left[M_{12}^{\mathrm{re}}\right]^2\rangle = \langle\left[M_{12}^{\mathrm{im}}\right]^2\rangle = \tfrac{1}{4}. \quad \text{(D13)}$$

These are half the variances of a GUE matrix, which is equivalent to a multiplication of each element of M by $1/\sqrt{2}$. This explains the rescaling of the coupling parameter in the definitions of $P_{4\to1}^1(s_1;\lambda)$ and $P_{4\to1}^2(s_2;\lambda)$, Eqs. (3.18) and (3.19).

For small N the argument in this section does not work. Presumably, this is the reason why the spacing distributions for the transition from GSE to GOE differ from those for the transition from GSE to GUE in the case of 4×4 matrices (not shown in this paper, but checked numerically), whereas they match very well for large matrices.

APPENDIX E: PERTURBATIVE CALCULATION OF THE RELATION BETWEEN EIGENVALUE DENSITY AND COUPLING PARAMETER

We consider a diagonal Poissonian matrix H_0 perturbed by a matrix taken from one of the Gaussian ensembles $H_{\beta'}$,

$$H = H_0 + \alpha H_{\beta'}, \quad \text{(E1)}$$

where $H_{\beta'}$ is chosen in the usual normalization [see Eq. (2.2)]. The calculations are done for arbitrary matrix dimension, which will be sent to infinity at the end. We denote the number of generically nondegenerate eigenvalues by N; i.e., we consider $N \times N$ matrices. If $H_{\beta'}$ is taken from the GSE, these are quaternion valued and correspond to complex $2N \times 2N$ matrices.

To obtain an N-independent eigenvalue density of the Poissonian ensemble, we define the probability distribution of the individual eigenvalues θ_i of H_0 by

$$\mathcal{P}_0(\theta_i) = \frac{1}{N}\hat{\mathcal{P}}_0(\theta_i/N), \quad \text{(E2)}$$

where $\hat{\mathcal{P}}_0$ is some N-independent probability distribution. Both $\mathcal{P}_0$ and $\hat{\mathcal{P}}_0$ are normalized to one. The eigenvalue density of the Poissonian ensemble is thus

$$\rho_0(\theta) = N\mathcal{P}_0(\theta) = \hat{\mathcal{P}}_0(\theta/N) = \hat{\mathcal{P}}_0(\hat{\theta}), \quad \text{(E3)}$$

where we have defined $\hat{\theta} = \theta/N$. Generically, we have $\theta_i = O(N)$ and $\hat{\theta}_i = O(1)$.

We now consider a fixed spacing S between two adjacent eigenvalues of H_0, θ_1 and $\theta_2 = \theta_1 + S$. The remaining eigenvalues have to reside outside the interval (θ_1, θ_2). This results in the conditional probability distribution

$$\mathcal{P}_0^{\mathrm{out}}(\theta_i) = \frac{1}{N}\hat{\mathcal{P}}_0^{\mathrm{out}}(\theta_i/N)$$

$$= \begin{cases} 0 & \text{for } \theta_i \in (\theta_1, \theta_2), \\ \frac{\mathcal{P}_0(\theta)}{1 - \int_{\theta_1}^{\theta_2} d\theta' \, \mathcal{P}_0(\theta')} & \text{otherwise.} \end{cases} \quad \text{(E4)}$$

The eigenvalue density is assumed to be almost unaffected by the perturbation, which is confirmed in Fig. 6 (top). Of course, this assumption is expected to hold only for small values of the coupling parameter.

We want to calculate the effect of the perturbation on the spacing S. If the remaining eigenvalues of H_0 are close to θ_1 or θ_2 we have to apply almost-degenerate perturbation theory. Up to second order in α we obtain for the perturbation of the spacing,

$$\Delta S = \underbrace{(\mathrm{EVD}[(H_0 + \alpha H_{\beta'})_{kl|\theta_k,\theta_l \in W}] - S)}_{\text{first-order almost-degenerate perturbation theory}}$$

$$+ \underbrace{\alpha^2 \sum_{i=3|\theta_i \notin W}^{N}\left(\frac{|(H_{\beta'})_{2i}|^2}{\theta_2 - \theta_i} - \frac{|(H_{\beta'})_{1i}|^2}{\theta_1 - \theta_i}\right)}_{\text{second-order perturbation theory}}, \quad \text{(E5)}$$

where the absolute values are taken with respect to the real, complex, or quaternionic standard norm, EVD denotes the difference of the two eigenvalues of the matrix $(H_0 + \alpha H_{\beta'})_{kl}$ that correspond to the unperturbed eigenvalues, and W is the interval in which eigenvalues have to be considered almost degenerate with θ_1 or θ_2. This is defined by the eigenvalue range $(\theta_1 - C_W, \theta_2 + C_W)$, where we choose $C_W = C_W^{(0)} N^\varepsilon \alpha$ with $0 < \varepsilon < 1$ and $C_W^{(0)} > 1$. This choice ensures that the closest possible eigenvalue outside W cannot give a second-order contribution of lower order in α than the

almost-degenerate part.[10] Note that the "degenerate window" W grows with N. Therefore arbitrarily distant eigenvalues are considered almost degenerate in the limit $N \to \infty$, which is justified because almost-degenerate perturbation theory is valid for any difference of eigenvalues.

Considering the first-order contribution, we have to deal with the matrix

$$M_{kl} = (H_0)_{kl} + \alpha(H_{\beta'})_{kl} = \theta_k \delta_{kl} + \alpha(H_{\beta'})_{kl}, \quad \text{(E6)}$$

where the indices k and l run over all values for which the eigenvalues θ_k and θ_l are localized in W, which includes at least θ_1 and θ_2. This is a matrix taken from the Poissonian ensemble perturbed by a matrix taken from one of the Gaussian ensembles, but unlike H defined in Eq. (E1) it has a constant eigenvalue density in the limit $N \to \infty$. To show this, we first consider the density at the lower end of the interval W,

$$
\begin{aligned}
\lim_{N \to \infty} N \mathcal{P}_0(\theta_1 - C_W) &= \lim_{N \to \infty} \hat{\mathcal{P}}_0 \left(\frac{\theta_1}{N} - \frac{C_W}{N} \right) \\
&= \lim_{N \to \infty} \hat{\mathcal{P}}_0 \left(\hat{\theta}_1 - C_W^{(0)} N^{\varepsilon - 1} \alpha \right) \\
&= \hat{\mathcal{P}}_0(\hat{\theta}_1) = \rho_0(\theta_1).
\end{aligned}
\quad \text{(E7)}
$$

This is the same as the eigenvalue density at the other end of W,

$$
\begin{aligned}
\lim_{N \to \infty} N \mathcal{P}_0(\theta_2 + C_W) &= \lim_{N \to \infty} \hat{\mathcal{P}}_0 \left(\frac{\theta_1}{N} + \frac{S + C_W}{N} \right) \\
&= \lim_{N \to \infty} \hat{\mathcal{P}}_0 \left(\hat{\theta}_1 + \frac{S}{N} + C_W^{(0)} N^{\varepsilon - 1} \alpha \right) \\
&= \hat{\mathcal{P}}_0(\hat{\theta}_1) = \rho_0(\theta_1).
\end{aligned}
\quad \text{(E8)}
$$

Thus the spectrum of M can be unfolded by multiplying with the local eigenvalue density,

$$\rho_0(\theta_1) M_{kl} = \underbrace{\rho_0(\theta_1) \theta_k \delta_{kl}}_{\text{unfolded}} + \underbrace{\alpha \rho_0(\theta_1)}_{\text{effective coupling}} (H_{\beta'})_{kl}. \quad \text{(E9)}$$

Therefore we can define a new effective coupling parameter that solely determines the magnitude of the perturbation as in Sec. III A.

The second-order contribution to ΔS in Eq. (E5) is a sum of at most $N - 2$ independent random numbers. As all of these random numbers have the same distribution we pick out one of them,

$$x = \alpha^2 \left(\frac{b}{\theta_2 - \theta_i} - \frac{a}{\theta_1 - \theta_i} \right) \quad \text{with} \quad \theta_i \notin W, \quad \text{(E10)}$$

---

[10] An eigenvalue $\theta_i = \theta_2 + C_W$ at the border of W yields a second-order shift of $\Delta \theta_2 = -\alpha^2 |(H_{\beta'})_{i2}|^2 / (C_W^{(0)} N^\varepsilon \alpha) = -\alpha |(H_{\beta'})_{i2}|^2 / (C_W^{(0)} N^\varepsilon)$.

where we defined $a = |(H_{\beta'})_{1i}|^2$ and $b = |(H_{\beta'})_{2i}|^2$. Its probability distribution is given by

$$
\begin{aligned}
\mathcal{P}_x(x) &= \left[\int_{-\infty}^{\theta_1 - C_W} + \int_{\theta_2 + C_W}^{\infty} \right] d\theta \frac{1}{N} \hat{\mathcal{P}}_0^{\text{out}}(\theta/N) \\
&\quad \times \int_0^\infty da\, db\, \mathcal{P}_{\beta'}(a) \mathcal{P}_{\beta'}(b)\, \delta \\
&\quad \times \left[x - \alpha^2 \left(\frac{b}{\theta_2 - \theta} - \frac{a}{\theta_1 \theta} \right) \right],
\end{aligned}
\quad \text{(E11)}
$$

where we renamed $\theta_i = \theta$ for convenience. The distribution $\mathcal{P}_{\beta'}$ depends on the symmetry class of the perturbing ensemble (a and b are squared sums of β' Gaussian random variables). The moments of this distribution are

$$p_m = \int_{-\infty}^{\infty} dx\, \mathcal{P}_x(x)\, x^m. \quad \text{(E12)}$$

After a short calculation, we obtain

$$
\begin{aligned}
p_m &= \int_{-\infty}^{0} d\theta \int_0^\infty da\, db\, \frac{1}{N} \left[\hat{\mathcal{P}}_0^{\text{out}} \left(\frac{\theta - C_W^{(0)} \alpha}{N} + \hat{\theta}_1 \right) \right. \\
&\quad \left. + \hat{\mathcal{P}}_0^{\text{out}} \left(\frac{S - \theta - C_W^{(0)} \alpha}{N} + \hat{\theta}_1 \right) \right] \mathcal{P}_{\beta'}(a) \mathcal{P}_{\beta'}(b) \\
&\quad \times \left[\alpha^2 \left(\frac{b}{S + C_W^{(0)} N^\varepsilon \alpha - \theta} - \frac{a}{C_W^{(0)} N^\varepsilon \alpha - \theta} \right) \right]^m.
\end{aligned}
\quad \text{(E13)}
$$

In the limit $N \to \infty$, all terms that are divided by N in the arguments of $\hat{\mathcal{P}}_0^{\text{out}}$ can be neglected. This can be done in spite of θ being integrated to ∞, because the last part of the integrand (in square brackets) suppresses the large-θ region and because $\hat{\mathcal{P}}_0^{\text{out}}$ is a probability density that has to converge to 0 for large argument. Also, $\lim_{N \to \infty} \hat{\mathcal{P}}_0^{\text{out}}(\hat{\theta}_1) = \hat{\mathcal{P}}_0(\hat{\theta}_1) = \rho_0(\theta_1)$. We thus obtain

$$
\begin{aligned}
p_m &= \frac{2\rho_0(\theta_1)}{N} \int_{-\infty}^{0} d\theta \int_0^\infty da\, db\, \mathcal{P}_{\beta'}(a) \mathcal{P}_{\beta'}(b) \\
&\quad \times \left[\alpha^2 \left(\frac{b}{S + C_W^{(0)} N^\varepsilon \alpha - \theta} - \frac{a}{C_W^{(0)} N^\varepsilon \alpha - \theta} \right) \right]^m.
\end{aligned}
\quad \text{(E14)}
$$

Let us denote the second line of Eq. (E5) by $\Delta S^{(2)}$. It is $O(N p_1)$, and therefore its mean value becomes zero for $N \to \infty$, as it is suppressed by $N^{-\varepsilon}$. The same holds for the second moment of $\Delta S^{(2)}$, which goes like $N^{-2\varepsilon}$. Thus the distribution of $\Delta S^{(2)}$ is a delta function at zero, and we can neglect its contribution to the perturbation of the spacing. The linear relation between eigenvalue density and coupling parameter could hence be shown up to second-order perturbation theory.

APPENDIX F: METHOD FOR FITS TO THE SURMISES

Since most of the analytical formulas for the small matrices contain integrals, it takes some time to compute them numerically. In order to get good fits to data in a reasonable time, a list of 1000 λ values in the interval $(0.01, 10)$ was created, with

$$\lambda_i = 0.01 \cdot 1000^{\frac{i-1}{999}}; \quad i = 1, \ldots, 1000. \quad \text{(F1)}$$

For each λ_i and each surmise, the corresponding spacing distribution was stored. The pure cases $\lambda = 0$ and $\lambda = \infty$ were included as well.

As a measure of the fit quality, we use the L_2 distance

$$\Delta_2 = \left\{ \int dx \, [f(x) - g(x)]^2 \right\}^{1/2} \tag{F2}$$

between the fit and the numerical data. The fitting was done by calculating the Δ_2 value of each spacing distribution in the list. From the one resulting in the smallest Δ_2 we read off the coupling λ. Note that the largest Δ_2 we encounter in all the fits is 0.019. For comparison, the L_2 norms of the pure Wigner surmises $P_\beta(s)$ range from 0.71 for $\beta = 0$ to 0.94 for $\beta = 4$. We give no error bars, because the statistical errors of λ obtained by methods such as the jackknife method were negligibly small. This is also the reason why we use Δ_2 instead of a statistical quantity like chi-squared as a measure of the fit quality.

APPENDIX G: CONSTRUCTION OF A SELF-DUAL GUE

In the following we construct a Hermitian, self-dual $2N \times 2N$ matrix whose eigenvalues are twofold degenerate and whose nondegenerate eigenvalues correspond to those of a matrix from the GUE. We start with a matrix M that contains an $N \times N$ GUE matrix H and its complex conjugate (equal to the transpose),

$$M = \begin{pmatrix} H & \mathbb{0}_N \\ \mathbb{0}_N & H^* \end{pmatrix}. \tag{G1}$$

The eigenvalues of M are obviously those of H, but now twofold degenerate as desired. However, M is not self-dual. To transform M into a self-dual matrix without changing its eigenvalues, we apply an orthogonal transformation

$$O = \begin{pmatrix} 1 & 0 & 0 & 0 & \cdots & 0 & 0 & 0 & 0 & 0 & 0 & \cdots & 0 & 0 \\ 0 & 0 & 0 & 0 & \cdots & 0 & 0 & 1 & 0 & 0 & 0 & \cdots & 0 & 0 \\ 0 & 0 & 1 & 0 & \cdots & 0 & 0 & 0 & 0 & 0 & 0 & \cdots & 0 & 0 \\ 0 & 0 & 0 & 0 & \cdots & 0 & 0 & 0 & 0 & 1 & 0 & \cdots & 0 & 0 \\ \vdots & \vdots & \vdots & \vdots & \ddots & \vdots & & \vdots & \vdots & \vdots & \vdots & \ddots & \vdots \\ 0 & 0 & 0 & 0 & \cdots & 1 & 0 & 0 & 0 & 0 & 0 & \cdots & 0 & 0 \\ 0 & 0 & 0 & 0 & \cdots & 0 & 0 & 0 & 0 & 0 & 0 & \cdots & 1 & 0 \\ 0 & 1 & 0 & 0 & \cdots & 0 & 0 & 0 & 0 & 0 & 0 & \cdots & 0 & 0 \\ 0 & 0 & 0 & 0 & \cdots & 0 & 0 & 0 & 1 & 0 & 0 & \cdots & 0 & 0 \\ 0 & 0 & 0 & 1 & \cdots & 0 & 0 & 0 & 0 & 0 & 0 & \cdots & 0 & 0 \\ 0 & 0 & 0 & 0 & \cdots & 0 & 0 & 0 & 0 & 0 & 1 & \cdots & 0 & 0 \\ \vdots & \vdots & \vdots & \vdots & \ddots & \vdots & & \vdots & \vdots & \vdots & \vdots & \ddots & \vdots \\ 0 & 0 & 0 & 0 & \cdots & 0 & 1 & 0 & 0 & 0 & 0 & \cdots & 0 & 0 \\ 0 & 0 & 0 & 0 & \cdots & 0 & 0 & 0 & 0 & 0 & 0 & \cdots & 0 & 1 \end{pmatrix} = O^T = O^{-1}, \tag{G2}$$

which transforms a matrix by exchanging every $2n$th row and column with the $(N + 2n - 1)$th one. Each of the four blocks is a square matrix of dimension N. This is in complete analogy to the construction of a self-dual 4×4 GUE matrix in Sec. II G.

We now show that the transformed matrix $O^T M O$ is self-dual, the condition for which is

$$O^T M O \stackrel{!}{=} J(O^T M O)^T J^T = J O^T M^T O J^T$$
$$\rightarrow M \stackrel{!}{=} O J O M^T O J^T O \tag{G3}$$

with

$$J = \mathbb{1}_N \otimes \begin{pmatrix} 0 & -1 \\ 1 & 0 \end{pmatrix}. \tag{G4}$$

Multiplying J by O from the left and the right interchanges the second, fourth, . . . with the $(N + 1)$th, $(N + 3)$th, ... column and row. We thus obtain

$$O J O = \begin{pmatrix} \mathbb{0}_N & -\mathbb{1}_N \\ \mathbb{1}_N & \mathbb{0}_N \end{pmatrix},$$

$$O J^T O = -O J O = \begin{pmatrix} \mathbb{0}_N & \mathbb{1}_N \\ -\mathbb{1}_N & \mathbb{0}_N \end{pmatrix}, \tag{G5}$$

and hence

$$O J O M^T O J^T O = \begin{pmatrix} \mathbb{0}_N & -\mathbb{1}_N \\ \mathbb{1}_N & \mathbb{0}_N \end{pmatrix} \begin{pmatrix} H^T & \mathbb{0}_N \\ \mathbb{0}_N & H \end{pmatrix} \begin{pmatrix} \mathbb{0}_N & \mathbb{1}_N \\ -\mathbb{1}_N & \mathbb{0}_N \end{pmatrix}$$

$$= \begin{pmatrix} H & \mathbb{0}_N \\ \mathbb{0}_N & H^T \end{pmatrix} = M, \tag{G6}$$

which proves Eq. (G3). $O^T M O$ can therefore be written as a quaternion matrix with real quaternions and their conjugates at the transposed position. Each of these quaternions stands for a matrix of the form

$$\begin{pmatrix} c_0 + i c_3 & c_1 + i c_2 \\ -c_1 + i c_2 & c_0 - i c_3 \end{pmatrix} = \begin{pmatrix} q & p \\ -p^* & q^* \end{pmatrix}, \tag{G7}$$

with complex numbers p and q. Evidently, p has to be zero for each quaternion in $O^T M O$, because our original M generically contains no element which is the negative complex conjugate of any other, and we only exchanged elements by applying O. This means that at least half of the matrix elements are zero. In the original M, exactly half of the matrix elements were zero, while the other half were random variables which depended on a total of N^2 real parameters, so the same has to hold for $O^T M O$. From this and Hermiticity if follows that every off-diagonal q has to be an independent complex random number, while the q on the diagonal are real, so that there are again N^2 real degrees of freedom.

With this equivalence proven, one can construct a self-dual GUE matrix by taking a matrix from the GSE and set its c_1 and c_2 components to zero. This matrix has the same joint probability density of the eigenvalues as an $N \times N$ matrix taken from the GUE, as it is related to a matrix of the form of M by a fixed basis transformation.

[1] T. Guhr, A. Müller-Groeling, and H. A. Weidenmüller, Phys. Rep. **299**, 189 (1998).

[2] J. Verbaarschot and T. Wettig, Annu. Rev. Nucl. Part. Sci. **50**, 343 (2000).

[3] G. Akemann, J. Baik, and P. Di Francesco (eds.), *The Oxford Handbook of Random Matrix Theory* (Oxford University Press, Oxford, 2011).

[4] T. A. Brody, J. Flores, J. B. French, P. A. Mello, A. Pandey, and S. S. M. Wong, Rev. Mod. Phys. **53**, 385 (1981).

[5] M. L. Mehta, *Random Matrices*, 3rd ed. (Elsevier/Academic, Amsterdam, 2004).

[6] R. Grobe, F. Haake, and H.-J. Sommers, Phys. Rev. Lett. **61**, 1899 (1988).

[7] G. Akemann, E. Bittner, M. J. Phillips, and L. Shifrin, Phys. Rev. E **80**, 065201 (2009).

[8] E. P. Wigner, Oak Ridge National Laboratory Report No. 2309, 1957, p. 59. (unpublished)

[9] O. Bohigas, M. J. Giannoni, and C. Schmit, Phys. Rev. Lett. **52**, 1 (1984).

[10] I. Dumitriu and A. Edelman, J. Math. Phys. **43**, 5830 (2002).

[11] T. Cheon, T. Mizusaki, T. Shigehara, and N. Yoshinaga, Phys. Rev. A **44**, R809 (1991).

[12] T. Shigehara, N. Yoshinaga, T. Cheon, and T. Mizusaki, Phys. Rev. E **47**, R3822 (1993), .

[13] A. Csordás, R. Graham, P. Szépfalusy, and G. Vattay, Phys. Rev. E **49**, 325 (1994).

[14] A. Y. Abul-Magd, B. Dietz, T. Friedrich, and A. Richter, Phys. Rev. E **77**, 046202 (2008).

[15] G. Lenz and F. Haake, Phys. Rev. Lett. **67**, 1 (1991).

[16] P. Shukla and A. Pandey, Nonlinearity **10**, 979 (1997).

[17] J. Sakhr and J. M. Nieminen, Phys. Rev. E **72**, 045204 (2005).

[18] D. Wintgen and H. Friedrich, Phys. Rev. A **35**, 1464 (1987).

[19] J. Goldberg, U. Smilansky, M. V. Berry, W. Schweizer, G. Wunner, and G. Zeller, Nonlinearity **4**, 1 (1991).

[20] B. I. Shklovskii, B. Shapiro, B. R. Sears, P. Lambrianides, and H. B. Shore, Phys. Rev. B **47**, 11487 (1993).

[21] P. Shukla, J. Phys.: Condens. Matter **17**, 1653 (2005).

[22] F. J. Dyson, J. Math. Phys. **3**, 1191 (1962).

[23] E. Follana, C. Davies, and A. Hart, PoS LAT **2006**, 051 (2006).

[24] A. M. García-García and J. C. Osborn, Phys. Rev. D **75**, 034503 (2007).

[25] T. G. Kovács, Phys. Rev. Lett. **104**, 031601 (2010).

[26] F. Bruckmann, T. G. Kovács, and S. Schierenberg, Phys. Rev. D **84**, 034505 (2011).

[27] M. V. Berry and M. Robnik, J. Phys. A **17**, 2413 (1984).

[28] M. S. Hussein and M. P. Pato, Phys. Rev. Lett. **70**, 1089 (1993).

[29] J. M. Nieminen, J. Phys. A: Math. Theor. **42**, 035001 (2009).

[30] T. A. Brody, Lett. Nuovo Cimento **7**, 482 (1973).

[31] M. V. Berry and P. Shukla, J. Phys. A **42**, 485102 (2009).

[32] T. Guhr, Ann. Phys. (NY) **250**, 145 (1996).

[33] H. Kunz and B. Shapiro, Phys. Rev. E **58**, 400 (1998).

[34] V. K. B. Kota and S. Sumedha, Phys. Rev. E **60**, 3405 (1999).

[35] M. Abramowitz and I. A. Stegun, *Handbook of Mathematical Functions*, 9th Dover ed. (Dover, New York, 1964).

[36] M. Robnik, J. Phys. A: Math. Gen. **20**, L495 (1987).

[37] H. Hasegawa, H. J. Mikeska, and H. Frahm, Phys. Rev. A **38**, 395 (1988).

[38] E. Caurier, B. Grammaticos, and A. Ramani, J. Phys. A: Math. Gen. **23**, 4903 (1990).

[39] I. S. Gradshteyn and I. M. Ryzhik, *Table of Integrals, Series and Products*, 5th ed. (Academic, San Diego, 1994).

[40] K. Gottfried and T.-M. Yan, *Quantum Mechanics: Fundamentals*, 2nd ed. (Springer, New York, 2004).

[41] A. Pandey, Ann. Phys. (NY) **134**, 110 (1981).

[42] J. B. French, V. K. B. Kota, A. Pandey, and S. Tomsovic, Ann. Phys. (NY) **181**, 198 (1988).

[43] J. Walker, *Fourier Analysis* (Oxford University Press, Oxford, 1988).